ERROR ANALYSIS, DESIGN THEORY, AND FAVORABLE OPERATIONAL CONDITION OF ELECTRONIC ANALOG MULTIPLIERS AND DIVIDERS

YASUJI MIYAKE and MAHITO ICHIKAWA

Depertment of Electrical Engineering

(Received June 7, 1971)

1. Introduction

Analog computers have a capability or at least a potentiality of handling straightforward many nonlinear problems occuring in engineering and physics as well as linear problems.

In solving such nonlinear problems, however, the multiplier plays the principal role, and hence studies for multipliers of higher performance have been made by many investigators and the number of types of multipliers published so far probably exceeds fifty[1].

This seems to indicate how much realizing multipliers of high performance comparable to that of linear computing elements was difficult.

We can divide analog multipliers into two classes; (a) the multipliers refered to the average-type multiplier, which have a low-pass or averaging filter in their output stage, such as the time-division multiplier, and (b) the multipliers refered to the instant-type multiplier, which can produce a product of inputs directly without filtering and which have a higher response speed, such as the diode multiplier.

On the other hand, the divider, almost without exception, is constructed by placing the multiplier in a negative feedback circuit or "β circuit" of an operational amplifier, as shown in Fig. 1.1. The feedback ratio of this circuit equals to the divisor Y and therfore this type of divider can be regarded as a variable-β system. As is well known, when the loop gain is sufficiently large, the gain defined by the ratio of input X to output Z is $-1/\beta = -1/Y$ and thus the division takes place.

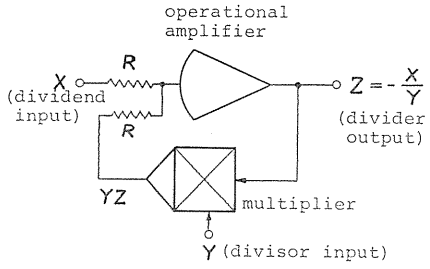

FIG. 1.1. Feedback-type analog divider.

Since also division is one of the basic arithmetic operation, the analog dividers can hardly be ignored in practical applications[2]. However, from the viewpoint of the differential analyzer, the analog divider was not necessarily an indispensable computing element in the early periode of analog computer development. For,

many differntial equations containing one or more division terms can be transformed into an equation without division term by multiplying both side members by an appropriate factor. Moreover at that time the multiplier yielding a divider with a sufficient accuracy, was not available (As discussed later on, the operational error of the divider is larger than that of the multiplier).

From this point of view, such a method using no divider was recommended[3] and analog dividers were rarely utilized, and hence there are virtully no reports concerning the operational characteristics of analog dividers. To the authors' knowledge, Numakura's study on the static characteristics of servo divider[4] is the only related paper.

However, unlike the early periode, as analog computers or more general analog techniques are widely used, it began to be noticed that the cases where the use of dividers is nessesary or desirable unexpectedly often occurs. This promoted the necessity of the error analysis of dividers for design and practical use, and led the authors to invesigate the problems treated in this paper.

1.1. The average-type multiplier

In spite of the fact that many types of multipliers have been divised, the multipliers of this type which have attained a wide use in analog computers are restricted to the time-division multiplier and the triangular-wave multiplier. The static error analysis of this class of multipliers belongs to the ordinary electronic circuit analysis of today, and hence is not included here. The dynamic characteristics of the multiplier are determined largely by the output low-pass filter and slightely by the modulation principle on which the multiplier is based. Although problems concerning this were investigated qualitatively by many workers and also by the authors, again this paper does not deal with them.

The static error of the divider was clearified by the authors by means of a graphical solution[5].

Since the average-type multiplier has no sufficient margin of dynamic response speed even for a slow type analog coputer, however, the divider derived from this type of multiplier may produce rather large dynamic errors and hence the analysis of this is required especially.

Nevertheless, since a divider is a two-input system with strong nonlinearity, the dynamic error varies greatly in amplitude and complexity depending on the operating conditions. Thus it is rather difficult to master the dynamic charecteristics of a divider with the concept of an ordinary linear computing element. Because of this, no proper method of designing and operating an analog divider has been formulated.

In Chapter 2, the authors set up the equations of motion for the dividers using the transfer functions of the related elements, and make quantitative and qualitative analysises of the dynamic characteristics of the dividers[5)~12)].

1.2. The instant-type multiplier

This type multipliers commonly used are restricted to the diode multipliers.

As is well known, the diode multiplier is based on the following identity, namely the "quarter squares principle"

$$(1/4)\{(x+y)^2-(x-y)^2\}=xy \tag{1.1}$$

where x and y are the inputs to be multiplied together, and therefore the basic unit of the multiplier is a squarer.

The typical diode squaring circuit is shown in Fig. 1.2. As the input voltage successively reaches critical values called breakpoints, another and another diode begin to conduct, switching additional parallel resistance into the circuit between the input and the summing point. Since the input-output characteristic is a straight-line approximation to the ideal parabolic characteristic, assuming that all the diodes have the ideal rectification characterestics, the maximim error of the squarer or multiplier is essentially determined by the numbers N of breakpoints contained in the positive dynamic range of the input voltage.

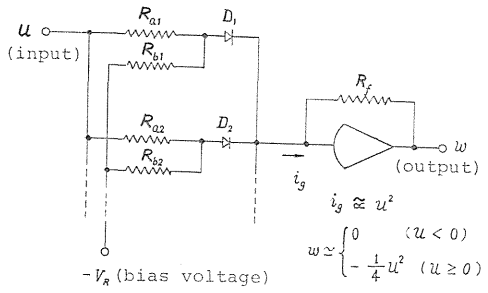

FIG. 1.2. Typical diode squaring circuit.

Since the multipliers of this type do not require tedious adjustmints and so severe compromise between response speed and the maximum static error in contrast to the average type multipliers, they are widely employed in the latest analog computers.

On the basis of the straight-line approximation to parabola, the diode multiplier exhibits a peculiar static error characteristic, and when the number N defined above is not large enough, or when the multiplier is operated at low level, or when the divider is constructed, several singular phenomena are experienced.

In Chapter 3, the static multiplication error is expressed as a function of two inputs x and y in a three dimensional form, assuming that the diodes have the ideal characteristic, and from this result the static division error in the same form can be derived[13)~16)].

Although these results are fairly useful for multipliers with a machine unit of 100 volts, the output characteristic of the multiplier in lower voltage, for example 10 volts, are strongly dependent on the actual voltage-current characteristics of the diodes. The design of such a multiplier seems to have been made individually for each given specification. Although experimental study on some special cases has been reported, some doubtful conclusions are found[17)~18)].

For these reasons the authors have investigate the existence of the data and the design theory applicable to every specification. The results are described concisely[19)~21)].

Chapter 4 is devoted to the problem: "How is the computer solution affected by the errors of multipliers or dividers in the computer circuit?" In the case of diode multiplier, the computer solution errors for typical differential equations are examined by the describing-function method or by simulating the analog computer circuits by a digital computer, and fairly general interpretation on the mechanisms of the error propergation from multipliers or dividers to the computer solution are presented[15)16)]. Also the relative merits of the diode multiplier and the average-type multiplier in solving a differential equation are discussed with several interesting results[13)25)].

2. Dynamic Errors of Feedback-type Electronic Analog Dividers

2.1. Equivalent circults of dividers

Two feedback-type analog dividers are shown in Fig. 2.1: (a) using high gain amplifier and multiplier, (b) using adder, sign changer and multiplier. These dividers can be represented by the general equivalent circuit shown in Fig. 2.2. From the feedback loops in Fig. 2.1, we have

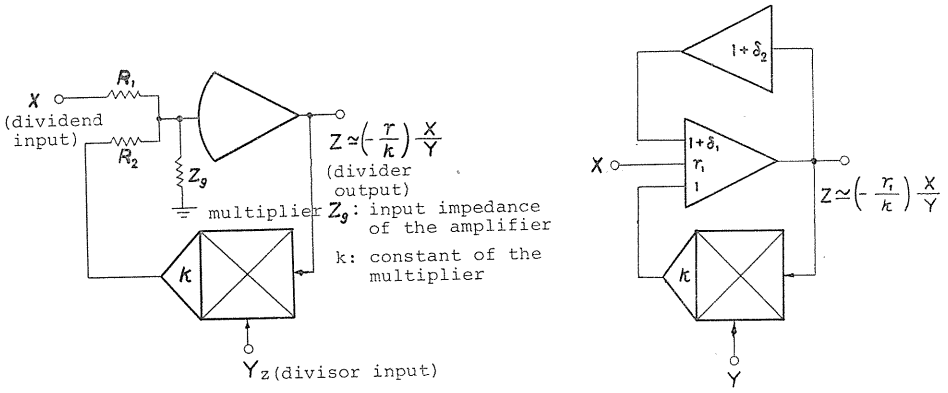

(a) Dvider using high gain amplifier. (b) Divider using adder and sign changer.

FIG. 2.1. Typical arrangements of electronic analog dividers.

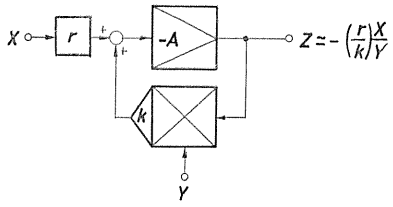

FIG. 2.2. General equivalent circuit of the dividers employing reciprocal multiplication.

for (a)

$$\left.\begin{aligned} r &= R_2/R_1 \\ A_e &= A/(1+R_2/R_1+R_2/Z_g) \end{aligned}\right\} \tag{2.1}$$

and for (b)

$$\left.\begin{aligned} r &= r_1 \\ A_e &= -1/(\delta_1+\delta_1\delta_2+\delta_2) \end{aligned}\right\} \tag{2.2}$$

In Fig. 2.1 (b), δ_1 and δ_2 are introduced for the purpose of evaluating the deviations of the coefficient of the No. 1 input of the adder and the coefficient of the sign changer from unity.

(The deviation of the coefficient of the No. 3 input of the adder from unity is included in k).

2.2. Equation of motion

The equivalent circuit of an actual multiplier is assumed to have linear elements connected to the inputs and outputs of an ideal multiplier as shown in Fig. 2.3 (b). Since we are interested in the dynamic characteristics, the spare nonlinearities in each of the blocks are neglected (which are important in determining the static characteristics).

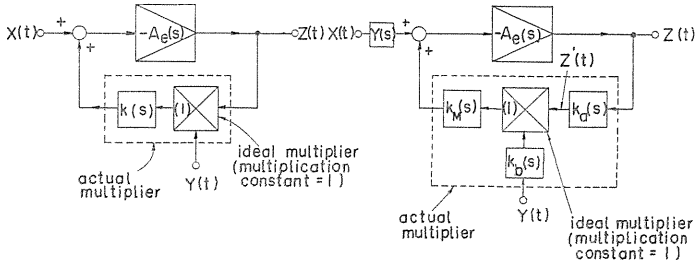

FIG. 2.3. Equivalent circuit for considering the dynamic characteristics of the dividers.

Since the output of a linear element with transfer function $K(s)$ and input $F_i(t)$ (*i.e.*, $E_0(t)=L^{-1}\{K(s)E_i(s)\}$) may be considered as the result of the operation of the linear operator $K(s)$ on the input $E_i(t)$, we shall represent the operation as $K*E_i(t)$. The operator K has the following properties.

(1) The inverse operation K^{-1} of the operator K, which makes $K^{-1}*K=K*K^{-1}=1$, is the operator with the transfer function $1/K(s)$.

(2) The operator having the property $K_1*K_2=K_2*K_1$ is the operator with the transfer function $K_1(s)*K_2(s)$. Using these operators, we obtain the expression for the feedback loop of Fig. 5 (a) as follows:

$$-A_e*\{(k*YZ)+X\}=Z \tag{2.3}$$

Operating both sides of the above equation with the operators A_e^{-1} and k^{-1} in succession, we obtain

$$(kA_e)^{-1}*Z+YZ=-k^{-1}*X \tag{2.4}$$

or

$$Y^{-1}(kA_e)^{-1}*Z+Z=-\frac{k^{-1}*X}{Y}\equiv Z_s' \tag{2.4'}$$

We shall call Eq. (2.4) or Eq. (2.4′) the equation of motion of the divider.

In Fig. 2.3 (b), since the elements $r(s)$ and $k_b(s)$ are not in the feedback loop, we may consider their output as $X(t)$ and $Y(t)$ and include $k_a(s)$ in $-A_e(s)$ and consider $Z'(t)$ as the output of the divider. In so doing, we obtain the same equivalent circuit as Fig. 2.3 (a) [the real output $Z(t)$ can be obtained directly from $(Zt)=k_a^{-1}*Z'(t)$]. Henceforth we shall proceed the analysis based on the circuit of Fig. 2.3 (a).

2.1. Transformation of an equation of motion

As long as the frequency range of X is within the operating frequency range of the multiplier, $k^{-1}*X \simeq k_0^{-1}X[k_0 = k(s)|_{s=0} = k(0) = DC$ value of the multiplication constant], and hence $Z_s' = -(k^{-1}*X)/Y$ is nearly an ideal quotient, and is corresponding to the forcing function of a differential equation. We shall call Z_s' the quasi-ideal quotient in later chapters.

Using Z_s', we define a quasi-division error ε' by

$$\varepsilon' = Z - Z_s' = Z - (-k^{-1}*X)/Y \tag{2.5}$$

By the use of Eq. (2.5), Eq. (2.2) transforms into the equation with ε' as unknown function. That is,

$$(kA_e)^{-1}*\varepsilon' + Y\varepsilon' = -(kA_e)^{-1}*Z_s' \tag{2.6}$$

Furthermore denoting the true ideal quotient by Z_s and defining the true division error ε by

$$\varepsilon' = Z - Z_s = Z - (-k_0^{-1}X/Y) \tag{2.7}$$

and substituting Eq. (2.7) into Eq. (2.2) lead to the following:

$$\left.\begin{aligned} &(kA_e)^{-1}*\varepsilon + Y\varepsilon = k_\varepsilon^{-1}*(YZ_s) - (kA_e)^{-1}*Z_s \\ \text{where}\quad &k_\varepsilon^{-1} = (k_0/k) - 1 \end{aligned}\right\} \tag{2.8}$$

As is seen from the discussion above, even if we choose any of Z, ε, ε' (or ε_0, ε_k, ε_k' defined in Sect 2.5.3) as an unknown function, we can write the equation of motion in the following form.

$$\left.\begin{aligned} &L*y(t) = f(t) \\ \text{where}\quad &L = (kA_e)^{-1} + Y \end{aligned}\right\} \tag{2.9}$$

and the unknown function $y(t)$ and the time-variable function $f(t)$ are given by Table 2.1.

TABLE 2.1. Different forms of the equation of motion
$L*y(t)=f(t)$ $\{L=(kA_e)^{-1}+Y\}$

$y(t)$	$f(t)$
divider output Z	$-k^{-1}*X = Y\cdot Z_s' = k_N^{-1}*(Y\cdot Z_s)$
division error ε	$k_\varepsilon^{-1}*(Y\cdot Z_s) - (kA_e)^{-1}*Z_s$
quasi division error ε'	$-(kA_e)^{-1}*Z_s'$
basic division error ε_0	$-(kA_e)^{-1}*Z_s$
ε_k'	$-(kA_e)^{-1}*\left(-\dfrac{k_{\varepsilon N}^{-1}*X}{Y}\right) = -(kA_e)^{-1}*\left\{\dfrac{k_\varepsilon^{-1}*(Y\cdot Z_s)}{Y}\right\}$
ε_k	$-\dfrac{k_{\varepsilon N}^{-1}*X}{Y} = \dfrac{k_\varepsilon^{-1}*(Y\cdot Z_s)}{Y}$ (where $L=1$)

Note: $k_N^{-1}=k_0/k$, $k_\varepsilon^{-1}=(k_0/k)-1$, $k_{\varepsilon N}^{-1}=k^{-1}-k_0^{-1}$

2.4. Series solution

If the waveform of Y is not restricted, the series solution of Eq. (2.9) may become difficult. Therfore, we assume Y has the functional form of Eq. (2.10).

$$Y = a + b\cos\omega t \tag{2.10}$$

Usually, in a feedback-type divider, the divisor is confined in the first quadrant. Here, if we assume $Y>0$, then it is nessessary that $a>0$, $b\geq 0$, $a-b>0$, $a+b\leq Y_r$, where Y_r is the maximum allowable divisor input of the divider.

Since the left-hand and right-hand sides of Eq. (2.9) are linear with respect to $y(t)$ and Z_s (or Z_s') respectively, we may assume, without loss of generality, that Z_s (or Z_s') is sinusoidal, *i.e.*

$$Z_s \text{ (or } Z_s') = \cos(\omega_1 t + \delta) \tag{2.11}$$

2.4.1. Case of $\omega_1 = n\omega$ (n = nonnegative integer)

In Eq. (2.9), let $y(t)$ be

$$y(t) = A_0 + \sum_{k=1}^{\infty} A_k \cos(k\omega + \theta_k) \tag{2.12}$$

Substituting this and Eq. (2.10) ($\omega_1 = n\omega$) and Eq. (2.11) into Eq. (2.9) and comparing the coefficients of like terms of the both sides, we obtained the following equations:

$$\left.\begin{aligned}
&\{G(0)+a\}y_0 + (b/2)y_1 = d_0 \\
&-P_1x_1 + by_0 + q_1y_1 + (b/2)y_2 = d_1 \\
&Py_1 + q_1x_1 + (b/2)x_2 = c_1 \\
&-P_kx_k + (b/2)y_{k-1} + q_ky_k + (b/2)y_{k+1} = d_k \\
&P_ky_k + (b/2)x_{k-1} + q_kx_k + (b/2)x_{k+1} = c_k \\
&\qquad (k = 2, 3, 4, \ldots)
\end{aligned}\right\} \tag{2.13}$$

where

$$\left.\begin{aligned}
&y_0 = A_0 \\
&x_k = A_k \sin\theta_k,\ y_k = A_k\cos\theta_k \\
&p_k = G(k\omega)\sin\varphi(k\omega) \\
&q_k = a + G(k\omega)\cos\varphi(k\omega) \qquad (k = 1, 2, 3, \ldots) \\
&G(\omega) = |k(j\omega)\cdot A_e(j\omega)|^{-1},\ \varphi(\omega) = \angle\{k(j\omega)\cdot A_e(j\omega)\}^{-1}
\end{aligned}\right\} \tag{2.14}$$

In Eq. (2.13), the equations of d_k and c_k are obtained by comparing the coefficients of $\cos k\omega t$ terms and $\sin k\omega t$ terms, respectively and are given by Tables 2.2 and 2.3. The functions $G(\omega)$ and $\varphi(\omega)$ in Eq. (2.13) are, respectively, the magnitude and phase angle of $\{k(s)\cdot A_e(s)\}^{-1}$ at the angular frequency ω.

If we choose a sufficiently large integer N, and truncate the series of Eq. (2.12) at $k=N$, then Eq. (2.13) becomes a set of $2N+1$ simultaneous equations and can be solved by hand computation, or by a digital computer.

TABLE 2.2. $[Z_s=\cos(n\omega t+\delta)]$

$y(t)$	c_k	d_k
Z	$ag_N(n\omega)\sin\{\delta+\phi_N(n\omega)\}$ $(k=n)$ $(b/2)(1+\delta_{on})g_N\{(n\pm1)\omega\}$ $\sin[\delta+\phi_N\{(n\pm1)\omega\}]$ $(k=n\pm1)$ 0 $(1\leqq k\leqq n-2,\ k\geqq n+2)$	$ag_N(n\omega)\cos\{\delta+\phi_N(n\omega)\}$ $(k=n)$ $(b/2)(1+\delta_{on})g_N\{(n\pm1)\omega\}$ $\cos[\delta+\phi_N\{(n\pm1)\omega\}]$ $(k=n\pm1)$ 0 $(0\leqq k\leqq n-2,\ k\geqq n+2)$
ε	$-ag_\varepsilon(n\omega)\sin\{\delta+\phi_\varepsilon(n\omega)\}$ $-G(n\omega)\sin\{\delta+\varphi(n\omega)\}$ $(k=n)$ $-(b/2)(1+\delta_{on})g_\varepsilon\{(n\pm1)\omega\}$ $\sin[\delta+\phi_\varepsilon\{(n\pm1)\omega\}]$ $(k=n\pm1)$ 0 $(1\leqq k\leqq n-2,\ k\geqq n-2)$	$-ag_\varepsilon(n\omega)\cos\{\delta+\phi_\varepsilon(n\omega)\}$ $-G(n\omega)\cos\{\delta+\varphi(n\omega)\}$ $(k=n)$ $-(b/2)(1+\delta_{on})g_\varepsilon\{(n\pm1)\omega\}$ $\cos[\delta+\phi_\varepsilon\{(n+1)\omega\}]$ $(k=n\pm1)$ 0 $(0\leqq k\leqq n-2,\ k\geqq n+2)$
ε_0	$-G(n\omega)\sin\{\varphi(n\omega)+\delta\}$ $(k=n)$ 0 $(k\neq n)$	$-G(n\omega)\cos\{\varphi(n\omega)+\delta\}$ $(k=n)$ 0 $(k\neq n)$

Note: $g_N(\omega)=|k(j\omega)/k(0)|^{-1}$, $\phi_N(\omega)=\angle\{k(j\omega)/k(0)\}^{-1}$
$g_\varepsilon(\omega)=|1-k(0)/k(j\omega)|$, $\phi_\varepsilon(\omega)=\angle\{1-k(0)/k(j\omega)\}$
$\delta_{on}=\begin{cases}0 & (n=0)\\ n & (n\neq0)\end{cases}$

TABLE 2.3. $[Z'_s=\cos(n\omega+\delta)]$

$y(t)$	c_k	d_k
Z	$a\sin\delta$ $(k=n)$ $(b/2)\sin\delta$ $(k=n\pm1)$ 0 $(1\leqq k\leqq n-2,\ k\geqq n+2)$	$a\cos\delta$ $(k=n)$ $(b/2)(1+\delta_{on})\cos\delta$ $(k=n\pm1)$ 0 $(0\leqq k\leqq n-2,\ k\geqq n+2)$
ε'	$-G(n\omega)\sin\{\varphi(n\omega)+\delta\}$ $(k=n)$ 0 $(k\neq n)$	$-G(n\omega)\cos\{\varphi(n\omega)+\delta\}$ $(k=n)$ 0 $(k\neq n)$

Note: δ_{on} has the same meaning as that ofTable 2.2.

2.4.2. *General case*

When $\omega_1\neq n\omega$, we let

$$y(t)=F\cos(\omega_1 t+\gamma)+\sum_{k=1}^{\infty}[A_k\cos\{(k\omega+\omega_1)t+\alpha_k\}+B_k\cos\{(k\omega-\omega_1)t+\beta_k\}] \tag{2.15}$$

With this, a set of equations having a generalized form for Eq. (2.13) can be obtained.

$$\left.\begin{aligned}
&-p_f x_f+q_f y_f+(b/2)(y_{1+}+y_{1-})=d_0\\
&p_f y_f+q_f x_f+(b/2)(x_{1+}-x_{1-})=C_0\\
&-p_{k\pm}x_{k\pm}+q_{k\pm}y_{k\pm}+(b/2)\{y_{(k-1)\pm}+y_{(k+1)\pm}\}=d_{k\pm}\\
&p_{k\pm}y_{k\pm}+q_{k\pm}x_{k\pm}+(b/2)\{x_{(k-1)\pm}+x_{(k+1)\pm}\}=C_{k\pm}\\
&(k=1,\ 2,\ 3,\ \ldots)
\end{aligned}\right\} \tag{2.16}$$

where

$$\left.\begin{aligned}
&x_0 = \pm x_f, && y_{0\pm} = y_f \\
&x_f = F\sin\gamma, && y_f = F\cos\gamma \\
&x_{k+} = A_k\sin\alpha_k, && y_{k+} = A_k\cos\alpha_k \\
&x_{k-} = B_k\sin\beta_k, && y_{k-} = B_k\cos\beta_k \\
&p_f = G(\omega_1)\sin\varphi(\omega_1) \\
&q_f = a + G(\omega_1)\cos\varphi(\omega_1) \\
&p_{k\pm} = G(k\omega\pm\omega_1)\sin\varphi(k\omega\pm\omega_1) \\
&q_{k\pm} = a + G(k\omega\pm\omega_1)\cos\varphi(k\omega\pm\omega_1) \\
&G(\omega) = G(|\omega|) && (\omega<0) \\
&\varphi(\omega) = -\varphi(|\omega|) && (\omega<0)
\end{aligned}\right\} \qquad (2.17)$$

and $c_k's$ and $d_k's$ are given by Tables 2.4 and 2.5.

For sufficiently large integers M and N, $A_{M+1}\simeq 0$, $B_{N+1}\simeq 0$, and hence the number of equations becomes $2(N+M+1)$.

TABLE 2.4. $[Z_s=\cos(\omega_1 t+\delta)]$

$y(t)$	$c_k\pm$	$d_k\pm$
Z	$c_0=ag_N(\omega_1)\sin\{\delta+\psi_N(\omega_1)\}$ $(b/2)g_N(\omega\pm\omega_1)\sin\{\pm\delta+\psi_N(\omega\pm\omega_1)\}$ $(k=1)$ 0 $(k\geqq 2)$	$d_0=ag_N(\omega_1)\cos\{\delta+\psi_N(\omega_1)\}$ $(b/2)g_N(\omega\pm\omega_1)\cos\{\pm\delta+\psi_N(\omega\pm\omega_1)\}$ $(k=1)$ 0 $(k\geqq 2)$
ε	$c_0=-ag_\varepsilon(\omega_1)\sin\{\delta+\psi_\varepsilon(\omega_1)\}$ $-G(\omega_1)\sin\{\delta+\varphi(\omega_1)\}$ $-(b/2)g_\varepsilon(\omega\pm\omega_1)\sin\{\pm\delta+\psi_\varepsilon(\omega+\omega_1)\}$ $(k=1)$ 0 $(k\geqq 2)$	$d_0=-ag_\varepsilon(\omega_1)\cos\{\delta+\psi_\varepsilon(\omega_1)\}$ $-G(\omega_1)\cos\{\delta+\varphi(\omega_1)\}$ $-(b/2)g_\varepsilon(\omega\pm\omega_1)\cos\{\pm\delta+\psi_\varepsilon(\omega\pm\omega_1)\}$ $(k=1)$ 0 $(k\geqq 2)$
ε_0	$c_0=-G(\omega_1)\sin\{\varphi(\omega_1)+\delta\}$ 0 $(k\geqq 1)$	$d_0=-G(\omega_1)\cos\{\varphi(\omega_1)+\delta\}$ 0 $(k\geqq 1)$

Note: Here $g_N(\omega)$, $g_\varepsilon(\omega)$, $\psi_N(\omega)$, $\psi_\varepsilon(\omega)$ have the same meaning as those of Table 2.2, respectively; for $\omega<0$, we make the following promise: $g_N(\omega)=g_N(|\omega|)$, $g_\varepsilon(\omega)=g_\varepsilon(|\omega|)$, $\varphi_N(\omega)=-\varphi_N(|\omega|)$, $\varphi_\varepsilon(\omega)=-\varphi_\varepsilon(|\omega|)$.

TABLE 2.5. $[Z_s'=\cos(\omega_1 t+\delta)]$

$y(t)$	$c_k\pm$	$d_k\pm$
Z	$c_0=a\sin\delta$ $\pm(b/2)\sin\delta$ $(k=1)$ 0 $(k\geqq 2)$	$d_0=a\cos\delta$ $\pm(b/2)\cos\delta$ $(k=1)$ 0 $(k\geqq 2)$
ε'	$c_0=-G(\omega_1)\sin\{\varphi(\omega_1)+\delta\}$ 0 $(k\geqq 1)$	$d_0=-G(\omega_1)\cos\{\varphi(\omega_1)+\delta\}$ 0 $(k\geqq 1)$

2.5. Operational solution

Although series solution is rather accurate, it is very difficult to foresee the final result, and, hence, there are inconveniences in operating and designing a divider. Because of this, we shall obtain explicit expressions for the solutions of the equation of motion.

2.5.1. Case when X is constant and Y varies in steps

When

$$\left.\begin{aligned} &X = X_0 \ (DC \text{ value}) \\ &Y(t) = Y_1 + (Y_2 - Y_1)u(t) \\ &[u(t) \text{ step function}] \end{aligned}\right\} \tag{2.18}$$

if we express the output $Z(t)$ of the divider as

$$\left.\begin{aligned} &Z(t) = Z_2 + (Z_2 - Z_1)f(t) \\ &f(t) = \begin{cases} -1 (t<0) \\ 0 (t \to \infty) \quad \text{(if stable)} \end{cases} \end{aligned}\right\} \tag{2.19}$$

(where Z_1 and Z_2 are the respective steadystate outputs of the divider when $X = X_0$ and Y is Y_1 and Y_2) then $f(t)$ is a time function determined by Y_2 alone, and the solution of the equation of motion is given by Eq. (2.20)

$$\begin{aligned} Z = {} & Z_1 \\ & + \{1 + (Y_2 k_0 A_{e0})^{-1}\} D(Y_2) \\ & * (Z_2 - Z_1)u(t) \end{aligned} \tag{2.20}$$

where

$$\begin{aligned} D(Y_2) &= \{1 + (Y_2 k A_e)^{-1}\}^{-1} \\ A_{e0} &= A_e(s)|_{s=0} = A_e(0) \end{aligned}$$

In Eq. (2.20), if we assume $\{1+(Y_2 k_0 A_{e0})^{-1}\}$ of the second term on the right-hand side is equal to one (≈ 1), then this output is equivalent to the output of a feedback system with loop gain $\mu = k(s)A_e(s)Y_2$ and unity feedback when a step of $(Z_2 - Z_1)u(t)$ is applied at $t=0$.

Therefore, if Y_2 is small, the transition from Z_1 will be slow and smooth; but Y_2 is large, the system may become oscillatory because the stability margin is reduced [for example, see (5), (7), (8)].

2.5.2. Solution by using time-variable operators

Generally speaking, the exact analytic solution is very difficult to obtain, however, an approximated analytic solution may be given in a comparatively simple form.

Rewriting Eq. (2.4′), we have

$$\{1 + Y^{-1}(kA_e)^{-1}\} * Z = -\frac{k^{-1} * X}{Y} \equiv Z_s'$$

On the right-hand side, although X is operated by the operator k^{-1}, related to the frequency characteristics of the multiplier, the operation of division by Y is complete and is affected by the feedback loop characteristics (which characterize the dynamics of the divider). Therefore, we shall call Z_s' the quasi-ideal quotient. On the other hand, the operator $\{1+Y^{-1}(kA_e)^{-1}\}$ is a function of the loop gain kA_eY alone, and hence is considered attributable to the phenomena given rise by the feedback. We shall now define the inverse operator of the time-variable operator $\{1+Y^{-1}(kA_e)^{-1}\}$ as follows:

$$D(Y, s) \equiv \{1 + Y^{-1}(kA_e)^{-1}\}^{-1} \tag{2.21}$$

With this definition, the formal solution is given by

$$\begin{aligned} Z &= D(Y, s) * \left(-\frac{k^{-1} * X}{Y} \right) \\ &= D(Y, s) * Z_s' \end{aligned} \tag{2.22}$$

The operator $\{1+Y^{-1}(kA_e)^{-1}\}$ may be considered as an operator of a fixed transfer function at a given instant, however, since it includes a time variable, it is difficult to interpret the physical meaning of the inverse operator. As an approximate interpretation, $D(Y, s)$ may be considered as an operator which modulates each frequency component of Z_s' with an amplitude of $|1+Y(t)^{-1}(kA_e)^{-1}|\omega$ and a phase angle of $\angle\{1+Y(t)^{-1}(kA_e)^{-1}\}|\omega$ if Y is slowly varying. Adding the subscript T to the operator having such physical meaning, we have

$$Z \simeq D_T(Y, s) * Z_s'$$

where

$$D_T(Y, s) = [1/\{1 + (kA_eY)^{-1}\}]_T \tag{2.23}$$

The quasi-division error ε' is then given by

$$\begin{aligned} \varepsilon' &= Z - Z_s' = \{D(Y, s) - 1\} * Z_s' \\ &\equiv D_{\varepsilon'}(Y, s) * Z_s' \simeq D_{\varepsilon' T}(Y, s) * Z_s' \end{aligned} \tag{2.24}$$

where

$$D_{\varepsilon' T}(Y, s) = \{-1/(1 + kA_eY)\}_T.$$

For the circuit of Fig. 2.3 (b), the complete expression for Z is given in the following:

$$\left.\begin{aligned} Z &= k_a^{-1} * \{1 + (k_b * Y)^{-1}(k_M k_a A_e)^{-1}\}^{-1} \\ &\quad * \left\{ -\frac{k_M^{-1} * (r * X)}{k_b * Y} \right\} \\ &= k_a^{-1} * D_T'(Y, s) * \left\{ \frac{(k_M^{-1} r) * X}{k_b * Y} \right\} \end{aligned}\right\} \tag{2.25}$$

where $D_T'(Y, s) = [1 + \{k_a k_M (k_b * Y)\}^{-1}]_T^{-1}$.

As another example of formal solution, we may derive from Eq. (2.4) [instead of Eq. (2.4′)] the following:

$$Z=\{(kA_e)^{-1}+Y\}^{-1}*(-k^{-1}*X) \tag{2.26}$$

If we interpret the inverse operator as above, the dynamic effect of Y will be completely ignored [since $(kA_e)^{-1}$ modifies the amplitudes and phases of the frequency components of X], and hence it is improper for the analysis of dynamic error.

As will be seen in Sect. 2.6, Eqs. (2.23) and (2.24) provide sufficiently accurate solutions. Since these equations are expressed as simple functions of Y, Z_s' and the characteristics of the elements of the divider, a spectral decomposition of Z_s' makes the physical meanings of these equations easily understood. In the series solution, even if we assume X is sinusoidal instead of Z_s or Z_s', the expression of Z remains unchanged. However, in the approximate solution (operational solution), from the properties of the time-variable operator $\{(kA_e)^{-1}+Y\}^{-1}$, it seems inconvenient to have X decomposed into frequency components.

Other forms of expressions for ε' may be obtained from Eq. (2.12). Dividing both sides of Eq. (2.12) by Y and then making the approximation as before, we have

$$\varepsilon'\simeq -D_T(Y,s)*\left\{\frac{(kA_e)^{-1}*Z_s'}{Y}\right\} \tag{2.27}$$

Or, dividing both sides of Eq. (2.12) by $\{1+(k_0A_{e0}Y)^{-1}\}$ and then making approximation, we have

$$\varepsilon'\simeq -\left\{\frac{1+(k_0A_{e0}Y)^{-1}}{1+(kA_eY)^{-1}}\right\}_T*\left\{\frac{(kA_e)*Z_s'}{1+(k_0A_{e0}Y)^{-1}}\right\} \tag{2.28}$$

From Eq. (2.24), these equations may possibly provide good approximations, however, it is difficult to foresee the results.

2.5.3. $Z_s'(\varepsilon')$ and $Z_s(\varepsilon)$

The error ε (or Z) resulting from the specified Z_s and Y has clearer physical meaning than ε' (or Y) which results from the specified Z_s' and Y. Since we have been dealing with the latter from theoretical point of view, we now investigate the relation between the two.

The true division error ε can be expressed, using Eq. (2.24), as follows:

$$\begin{aligned}\varepsilon&=Z-Z_s=(Z-Z_s')+(Z_s'-Z_s)\\&=\varepsilon'+\varepsilon_k=\varepsilon_0+\varepsilon_k'+\varepsilon_k\end{aligned} \tag{2.29}$$

where

$$\varepsilon_0=D_{\varepsilon'}(Y,s)*Z_s\simeq -\left(\frac{1}{1+kA_eY}\right)_T*\left(-\frac{k_0^{-1}X}{Y}\right)$$

$$\varepsilon'=D_{\varepsilon'}(Y,s)*\left(-\frac{k_{\varepsilon N}^{-1}*X}{Y}\right)$$

$$\simeq -\left(\frac{1}{1+kA_eY}\right)_T*\left(-\frac{k_{\varepsilon N}^{-1}*X}{Y}\right)$$

$$\varepsilon=-\frac{k_{\varepsilon N}^{-1}*X}{Y}$$

$$k_{\varepsilon N}^{-1}=k^{-1}-k_0^{-1}$$

In the above, ε_0 is the error due to the feedback characteristic kA_eY only; ε_k is the error due to the characteristic of the multiplier k, only; and ε_k' is the error due to the multiplication effect of the above two characteristics. From the expression for ε_0, it is clear that when the waveforms of Z_s' and Y are, respectively, identical with that of Z_s and Y, ε' is equal to ε_0. Therefore, in order to obtain ε of the case of given (Z_s, Y) from ε' of the case of given (Z_s', Y), it is necessary to determine ε_k and ε_k'. When Z_s is sinusoidal, the evaluation of ε_k' is rather tedious. However, if the frequency spectrum of $(k_{\varepsilon N}^{-1}*X)/Y$ is concentrated in the frequency band where $|1+kA_eY| \gg 1$, then ε_k' may be neglected compared with ε_k.

As a means of improving dynamic characteristics, an element having transfer function $k_N(s)$ is inserted at the dividend input of the divider as shown in Fig. 2.11. In this case, the equation of motion becomes

$$Y^{-1}(kA_e)^{-1}*Z+Z=\frac{k^{-1}*(k_N*X')}{Y}$$
$$=-\frac{k_0^{-1}X'}{Y} \tag{2.30}$$

where $X=k_NX'$. Therefore, Z and ε' of the case of given (Z_s', Y) are exactly the same as Z and ε of the case of given (Z_s, Y).

2.5.4. Relation between (X, Y) input and Z_s'

From the nonlinear relation $Z_s'=-(k^{-1}*X)/Y$, it is observed that when Y is small, Z_s' varies steeply as Y is varied. An example is shown in Fig. 2.4 for the case $X=-k_0$ (constant). As will be clear later on, this steep variation of Z_s' is one of the main causes of the division error, and hence attention must be paid to the errors when Y is near its minimum. When the variation range of divisor is large (*i.e.*, when the ratio of the maximum to minimum of the divisor is large), because $Y_{\min}$ is small, Z_s' varies steeply in the vicinity of $Y=Y_{\min}$ even if the frequency band of Y is restricted. Expanding the waveform of Z_s' in Fig. 2.4, we have

$$Z_s'=\frac{1}{a+b\cos\omega t}$$
$$=\frac{1}{a\sqrt{1-m^2}}\{1+2\sum_{n=1}^{\infty}(-A)^n\cos n\omega t\} \tag{2.31}$$

where

$$A=\frac{1-\sqrt{1-m^2}}{m},\quad m=\frac{b}{a}$$

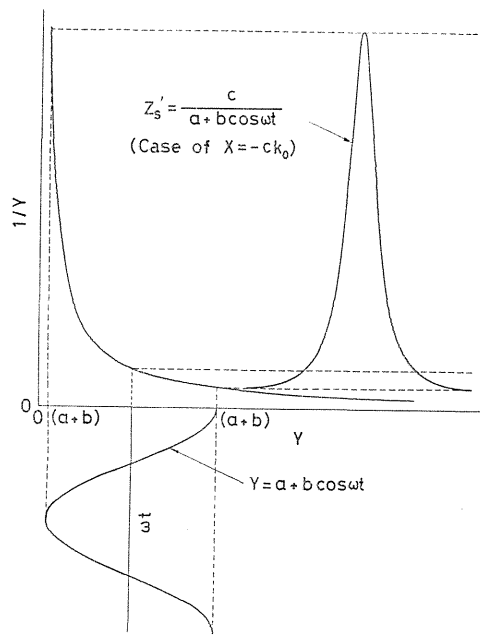

FIG. 2.4. Example of a steep variation of Z_s' based on the non-linear relation between Y and Z_s'.

If the variation range of Y is $Y_{\min}-Y_r$, and the minimum value of $Y=a+b\cos\omega t$ is $Y_{\min}$, then

$$m=\frac{1}{1+(Y_{\min}/b)} \tag{2.32}$$

Therefore, for a given b (the curvature of Y waveform is fixed if ω is fixed), if $Y_{\min}$ is small, $m\to 1$ and hence $A\to 1$. Thus, even if ω is within the practical frequency band of the multiplier, the frequency spectrum of Z_s' may easily spread beyond this band.

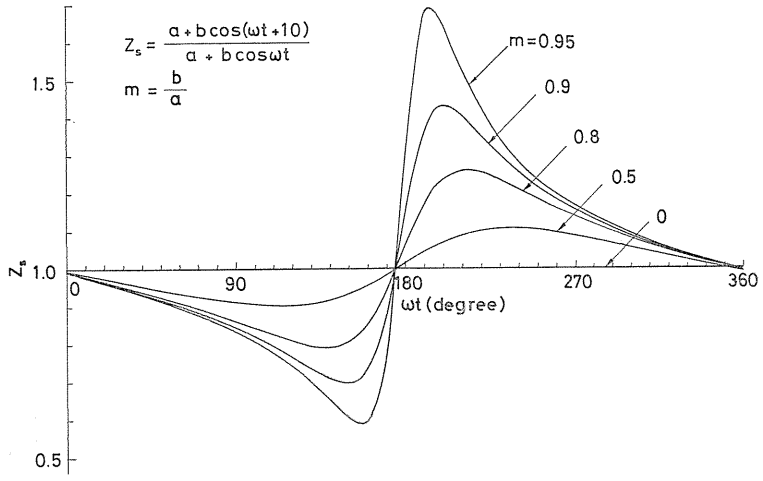

FIG. 2.5. Waveform of Z_s' in the case when $-k^{-1}*X=a+b\cos(\omega t+10°)$ and $Y=a+b\cos\omega t$.

In contrast to Fig. 2.4, when $-k^{-1}*X=Y=a+b\cos\omega t$, the effect of the nonlinear relation between Z_s' and Y disappears completely. However, this is merely a particular case, and can not be expected in general. For example, in Fig. 2.5, although there is only a 10-degree difference in phase between the numerator and denominator of Z_s', the variation of Z_s' is as steep as the case of Fig. 2.4 when Y is small.

2.6. Numerical calculation

2.6.1. Calculation method

As an example, we shall illustrate the manipulation of case (a) (1) in Sect. *2.4.1.* If we let $x_{N+1}=y_{N+1}=0$ in the two equations for $k=N$ in Eq. (2.13), then x_N and y_N can be expressed in terms of x_{N-1} and y_{N-1} in linear form. Substituting these expressions into the two equations for $k=N-1$, we obtain the expressions for x_{N-1} and y_{N-1} in terms of x_{N-2} and y_{N-2}. Repeating the same process, we finally obtain a set of simultaneous linear equations of three variables x_1, y_0, y_1. From this set of equations, we can determine x_1, y_0, y_1, and then determine x_2, y_2; x_3, y_3; $\cdots$, in succession.

In Eq. (2.13), if $c_k=d_k=0$ for $k\geq\mu$, then the relation between x_k, y_k and x_{k-1}, y_{k-1} obtained in the above manipulation becomes

$$\begin{pmatrix} x_k \\ y_k \end{pmatrix} = P_k \begin{pmatrix} x_{k-1} \\ y_{k-1} \end{pmatrix} \quad (k \geq \mu) \tag{2.33}$$

where

$$P_k = \begin{pmatrix} a_k & b_k \\ b_k & -a_k \end{pmatrix}$$

is an orthogonal matrix. Since A_k and θ_k are, respectively, the amplitude and phase angle of the vector (x_k, y_k), the amplitude ratios A_μ, $A_{\mu+1}$, $A_{\mu+2}$, ... ; A_N and the phase differences $(\theta_{\mu+1}-\theta_\mu)$, $(\theta_{\mu+2}-\theta_\mu)$, ... , $(\theta_N-\theta_\mu)$ are constants regardless of the values of x_μ and y_μ. Therefore, if Z_S is obtained for $\mu=\mu_1$, then, for the case of $\mu=\mu_2$ with the same ω, we need only to evaluate up to the max (μ_1, μ_2)-th A and θ.

In the approximation solution, the form of Y is not necessarily $a+b\cos\omega t$, and in particular, if Z_s' has a simple sinusoidal waveform (ω_1), the calculation becomes very simple. To obtain the amplitude and phase angle of $D_T(Y, \omega_1)$ or $D_{\varepsilon T}(Y, \omega_1)$ at each instant, the Nichols chart may be used.

2.6.2. Calculation results

For the caracteristics of the experimental divider, the characteristics of k and A_e shown in Fig. 2.6 will be used. Since the full-scale of Y in this experimental divider is 10 V, $a=5$ and $b=4.5$ are chosen for the case of large variation range of Y $(Y_{\max}/X_{\min}=19)$. For the frequency $f=\omega/2\pi$, 20 Hz is taken as a high fre-

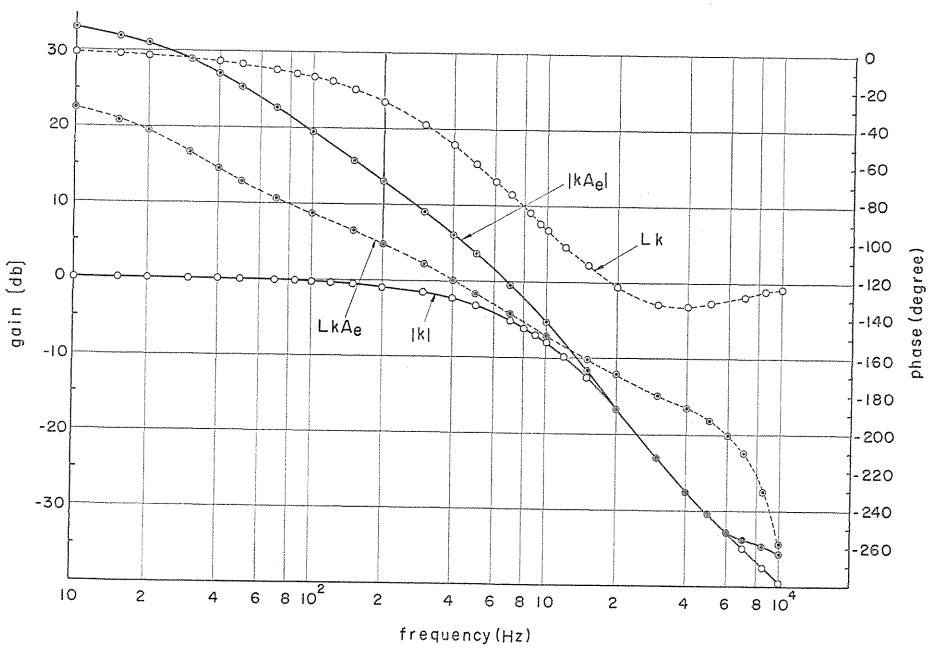

FIG. 2.6. Example of the frequency characteristics of k and kA_e.

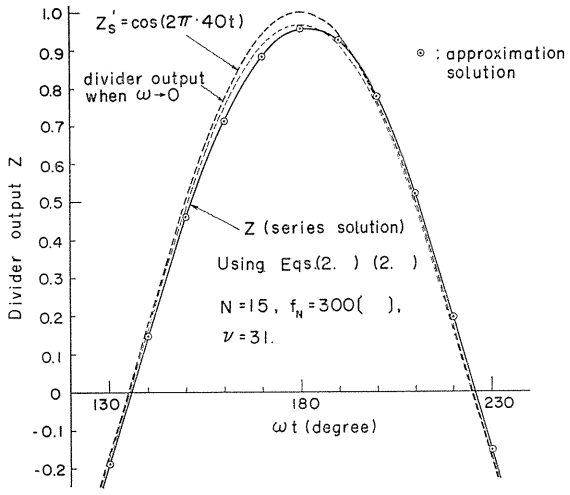

(a) Deviation of the real divider output Z from the quasi-ideal divider output.

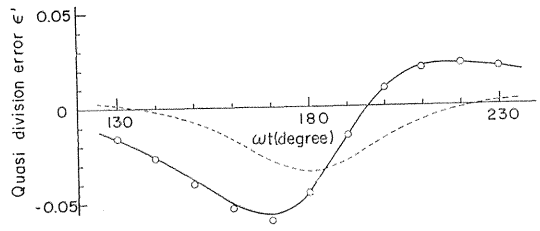

(b) Quasi-division error $\varepsilon' = Z - Z_s'$

FIG. 2.7. Response of the divider in the case when $Z_s' = \cos(2\pi 40t)$ and $Y = 5 + 4.5\cos(2\pi 20t)$.

quency within the practical frequency band of the multiplier (at which $\angle k \simeq -2°$), 300 Hz is a frequency outside of the practical frequency band.

The computation results by the series method and the approximation method are shown in Figs. 2.7–2.10, 2.13 and 2.14. In the series solutions, the highest frequency components of Z and $\varepsilon'(\varepsilon)$ are, respectively, denoted by M and N, and their corresponding frequencies by $f_N\{=(N_\omega+\omega_1)/2\pi\}$ and $f_M\{=(M_{\omega-\omega_1})/2\pi\}$, and the order of the simultaneous equations by ν.

(a) In the practical frequency range ($f=20$ Hz)

Figures 2.7–2.10 show that the approximate solutions are quite accurate when the operating frequency is within the practical frequency band of the multiplier. We shall interpret the computation results in the following.

Figures 2.7 and 2.8 show the examples related to Eq. (2.31) in which ω_1 is an integral multiple of ω. When ω_1 is the second harmonic of ω, *i.e.*, 40 Hz, (Fig. 2.7), $|D_T(Y, 2\omega)|$ is minimum at $\omega t = 180°$ and $\angle D_T(Y, 2\omega)$ is maximum (lagging). As a result, ε' increases in the neighborhood of $\omega t = 180°$. The static error ε', *i.e.*, the error when $\omega_1 = 2\omega \to 0$, is shown in Fig. 2.5 (b) by the dotted

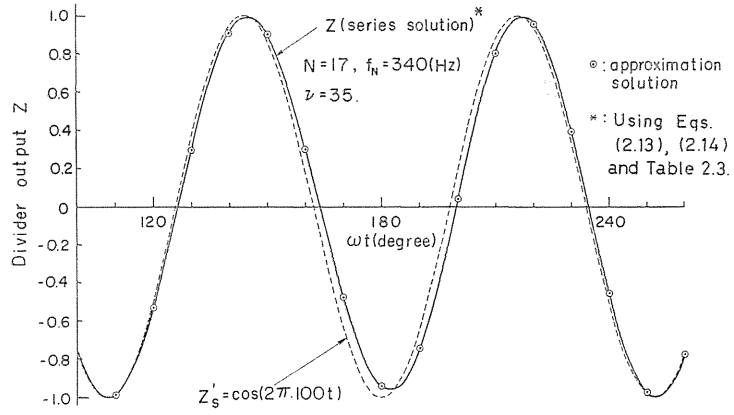

(a) Deviation of the real divider output Z from the quasi-ideal divider output Z'_s.

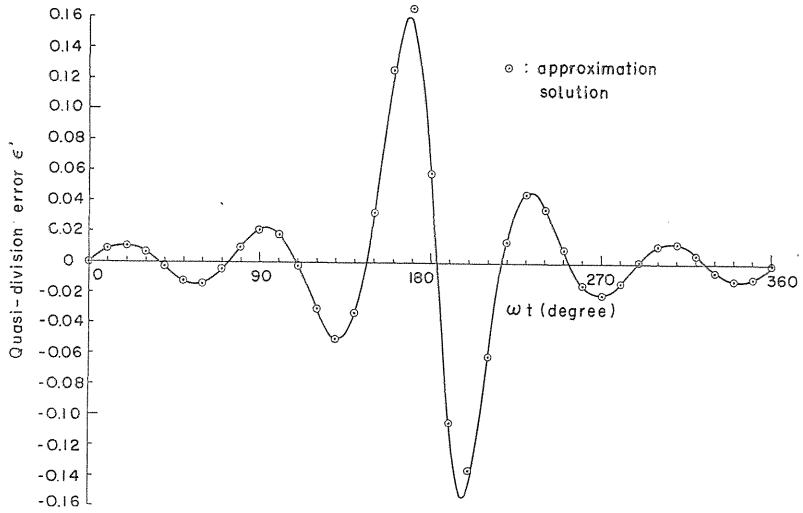

(b) Quasi-division error: $\varepsilon'=Z-Z'_s$

FIG. 2.8. Response of the divider in the case when $Z'_s=\cos(2\pi 100t)$ and $Y=5+4.5\cos(2\pi 20t)$.

line which is even-symmetrical about $\omega t=180°$. Because of the strong effect of $\angle D_T(Y, 2\omega)$, the dynamic error curve in this case becomes almost oddsymmetrical. When ω_1 is the fifth harmonic of ω, *i.e.*, $\omega_1=100$ Hz (Fig. 2.8) the above-mentioned tendency becomes more noticeable and the maximum error ε' reaches 16%.

Figure 2.9 shows the case where X is considered time dependent and ω_1 is 2.5 times ω. The effect of the phase difference δ between Y and Z'_s is also investigated. When $\delta=0°$, since Z'_s has a maximum slope in the vicinity of $\omega t=180°$ where $D_T(Y, 2.5\omega)$ is maximum, the peak of ε' becomes large and reaches about 10%. When $\delta=-60°$, since the slope of Z'_s is small in the vicinity of 180°, the

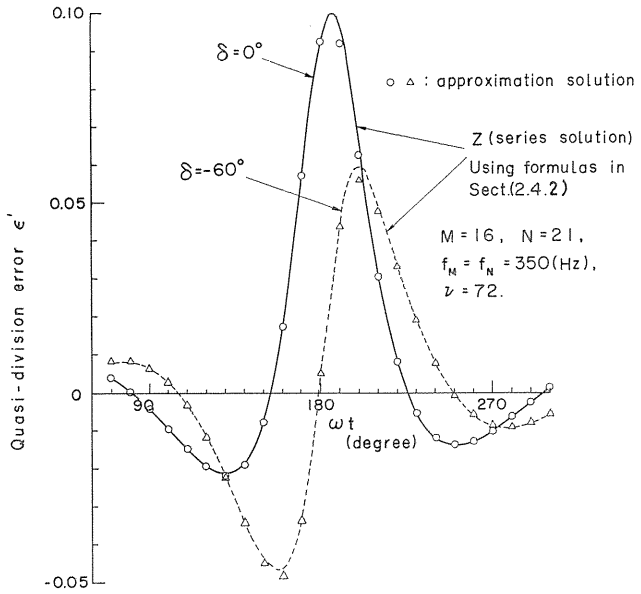

FIG. 2.9. Quasi division errors in the case when $Z_s'=\cos\{(2\pi 50t)+\delta\}(\delta=0°, -50°)$ and $Y=5+4.5\cos(2\pi 20t)$.

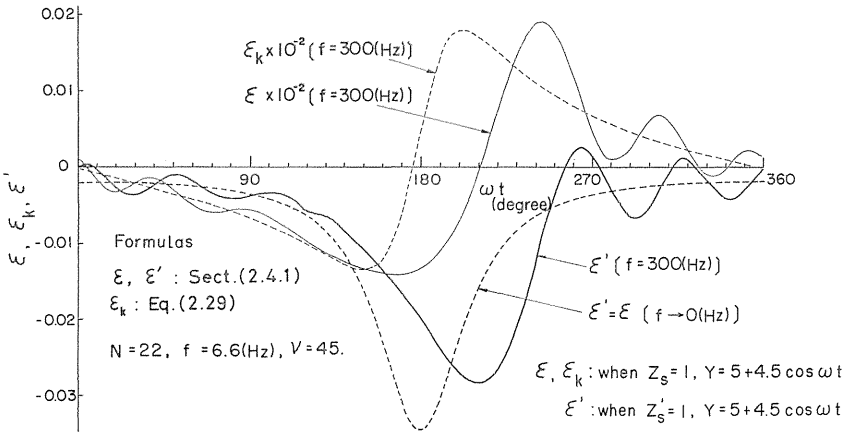

FIG. 2.10. (Quasi) division errors in the case when $Z_s(Z_s')=1$ and $Y=5+4.5\cos\omega t$.

peak of ε' is reduced to one half although $\angle D_T(Y, 2.5\omega)$ is about the same.

In summary: (1) ε' increases as the frequency spectrum inclines toward high-frequency ranges; (2) ε' increases as Y approaches its minimum; (3) the effect of phase difference between Z_s' and Y is also quite remarkable. From Sect. *2.5.4*, when the variation range of Y is large, both (1) and (2) are in effect, therefore, the division error becomes large.

(b) Outside the practical frequency range ($f=300$ Hz)

(1) $Z_s'=1\ (\omega_1=0)$

If the waveforms of X and Y are similar, the ideal solution must be a con-

stant independent of waveform. However, from the ε-curves for $Z_s=1$ in Fig. 2.10, it is observed that although the generated solution is nearly unity for $f=0$ Hz, the error curve for $f=300$ c/s has large ripples on it. This may be considered due to the A_e components in the forcing term $Z_s'=-(k^{-1}*X)/Y$ of the equation of motion which appears under the influence of k^{-1}. In fact, when $Z_s'=1$, the amplitude of the error is almost unchanged even if the frequency f is raised from 0 to 300 Hz.

Therefore, if we insert an element $k_N(s)$ in front of the X input as shown in Fig. 2.11, we should be able to eliminate the error mentioned above. The experimental result is shown in Fig. 2.12 (The ripple error at the low-frequency range is due to the static error of the multiplier). Since $k_N(s)$ is $k(s)/k(0)$, it is similar to the characteristics of the low-pass filter attached at the output terminals of a time-division multiplier. Consequently, by using the filter circuits having the same frequency characteristics in the frequency band of X, the compensation of error ripples can easily be realized. Moreover, if the output filter can be removed from the multiplier, then, by inserting this filter between the adder and the high-gain amplifier, we can attain the same compensation effect (This can not be done if the divider consists of adder and sign changer). In a divider utilizing the high-gain amplifier, $r(s)=1$. However, in a divider utilizing adder and sign-changer, $r(j\omega)$ is generally of low-pass characteristics; therefore, the effect of k^{-1} is partially suppressed [See Eq. (2.25)].

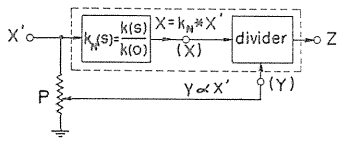

FIG. 2.11. A method for excluding $(\varepsilon_k+\varepsilon_k')$.

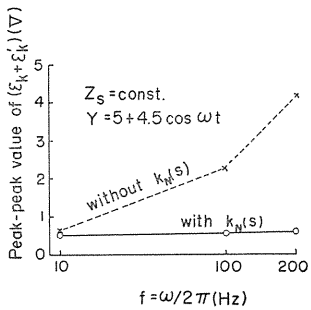

FIG. 2.12. Experimental values of $(\varepsilon_k+\varepsilon_k')$.

(2) $Z_s'=\cos(2\pi 600t)(\omega_1=2\omega)$

Fig. 2.13 shows an example such that when the variation of Y is fast, the approximation method does not provide accurate solution. In this case, although both Y and Z_s' are rapidly varying, the error curve ε' given by Eq. (2.24) is exactly the same as that for constant Z_s' shown by the dotted line in Fig. 2.10. This is far different from the actual error curve ε' shown by the solid line in the same figure.

(3) $Z_s'=1/\{5+4.5\cos(2\pi 300t)\}(\omega_1=0,\ \omega,\ 2\omega,\ \ldots)$

When Z_s' contains a number of sinusoidal components and X is sinusoidal or *DC*, the formula of Z for the case of sinusoidal Z_s' can be directly applied except that the expressions of c and d have to be modified. For $X=-k_0$, the right-hand side of Eq. (2.4′) $=-k^{-1}*X=1$, therefore,

$$\left.\begin{aligned} c_k &= 0 \qquad (k\geq 1)\\ d_k &= \begin{cases} 1 & (k=0)\\ 0 & (k\geq 1)\end{cases}\end{aligned}\right\} \tag{2.34}$$

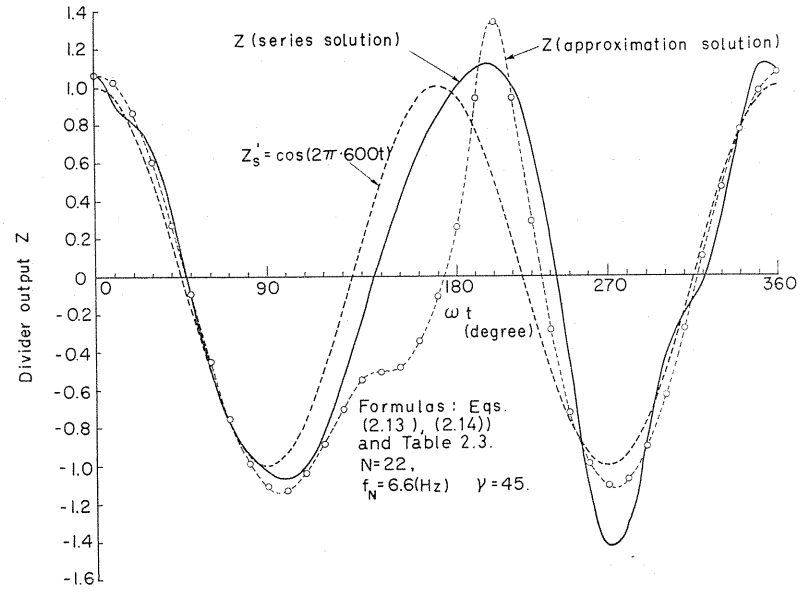

FIG. 2.13. Divider output in the case when $Z_s'=\cos(2\pi 600t)$ and $Y=5+4.5\cos(2\pi 300t)$.

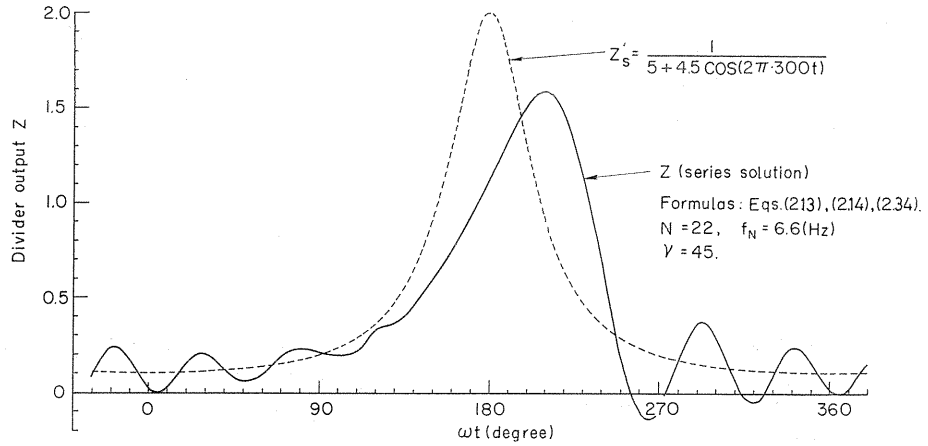

FIG. 2.14. Divider output in the case when $X=-k_0$ and $Y=5+4.5\cos(2\pi 300t)$ [c.f. FIG. 2.15 (d)].

The calculated Z is shown in Fig. 2.14 in which a high-frequency oscillation is observed. The oscillatory frequency is found to be about 2 kHz and is roughly equal to the frequency of the dominant characteristic roots of the feedback loop when Y is large.

2.6.3. Properties of approximation solutions outside of the practical frequency band

The inaccuracy of the approximation solution mentioned above is a natural

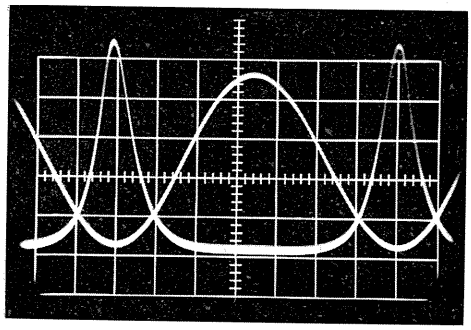

(a) $f=20$ (Hz), $a=5$ (V), $b=4.5$ (V); $Z_0=2.7$ (V); 1 (V/div).

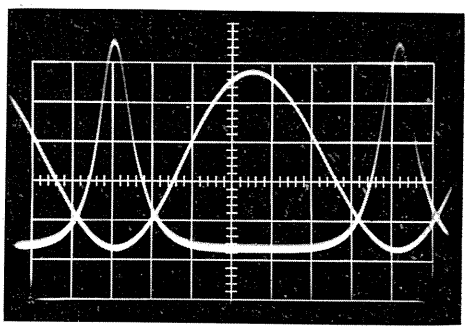

(b) $f=40$ (Hz), $a=5$ (V), $b=4.5$ (V); $Z_0=2.7$ (V); 1 (V/div).

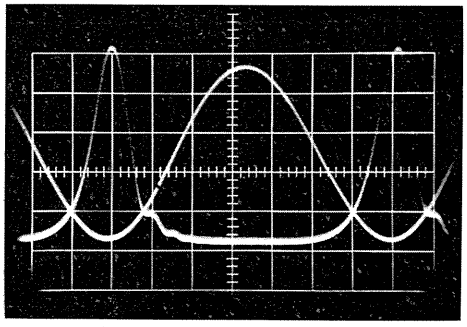

(c) $f=100$ (Hz), $a=5$ (V), $b=4.5$ (V); $Z_0=2.7$ (V); 1 (V/div).

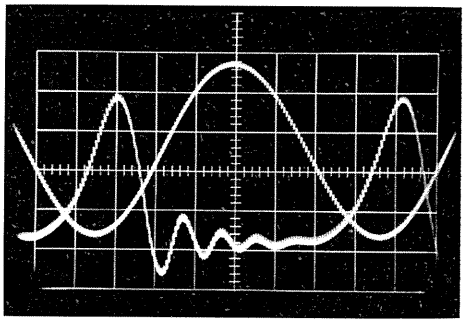

(d) $f=300$ (Hz), $a=5$ (V), $b=4.5$ (V); $Z_0=2.7$ (V); 1 (V/div).

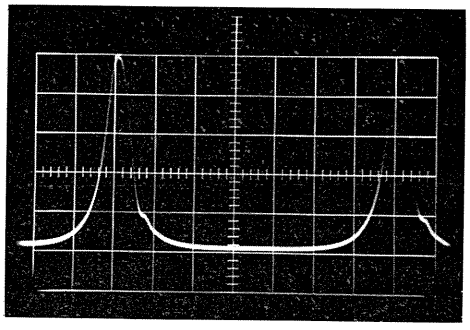

(e) $f=40$ (Hz), $a=4.85$ (V), $b=4.65$ (V); $Z_0=2.5$ (V).

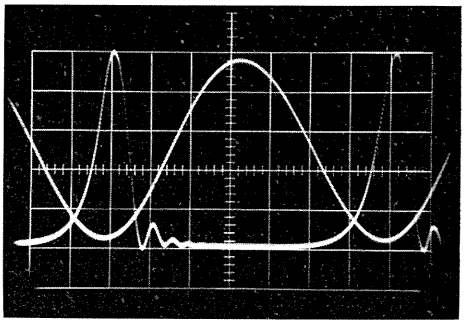

(f) $f=100$ (Hz), $a=4.85$ (V), $b=4.65$ (V); $Z_0=2.5$ (V).

FIG. 2.15. Waveforms of the divider output in the case when $X=Z_0$, $Y=a+b\cos\omega t$.

consequence of the approximation approach. Although inaccurate, the approximation solution serves to clarify the qualitative aspects of the computation results. For instance, in Fig. 2.14, Z_s' rises steeply when ωt approaches 180° (at which Y becomes $Y_{\min}$), but, because $|D_T(Y, j\omega)|$ at high frequency is very small, the rise of Z trails Z_s' by a large delay. When ωt exceeds 180°, Z_s' drops sharply, and hence Z starts to decrease. But, after this, Y is increased and a peak of $|D_T(Y, j\omega)|$ appears in the high-frequency range; therefore, an oscillatory Z is observed. Figures 2.15 (a)-(d) show the waveforms of Z for various ω when $X=$const, $Y=a+b\cos\omega t$. When ω is increased, the amplitude of the component of Z_s in the vicinity of the frequency of the dominant characteristic root is increased, and hence a larger oscillation is observed in the period where Y is large. Fig. 2.15 (d) corresponds to the case of Fig. 2.14. The two results agree with each other within the experimental error. Figures 2.15 (e) and (f) show the cases where b/a approaches 1 more closely ($b/a=0.9\rightarrow0.96$). This is another way of increasing the high-frequency component of Z_s. Note that the case of $f=100$ (Hz) has larger oscillation in Z.

2.7. Method of measuring division error

It is very difficult to measure the division error from the observation of Z, because the error itself is very small. As a solution to this problem, we shall describe a method in which only the quasi-division error is generated and amplified at the output of the divider proper.

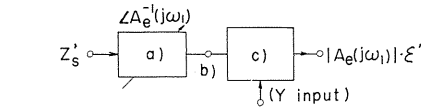

a) variable phase shifter (arbitrary)
b) x input
c) divider
for example : $Z_s'=A\cos(\omega t+\delta)$ amplitude
A can assume any value convenient for measuring.

FIG. 2.16. Principle of the method for observing the quasi division error ε'.

Rewriting the right-hand side of Eq. (2.6) as $-k^{-1}*(A_e^{-1}*Z_s')$, and comparing this with Eq. (2.4) we conclude that when $A_e^{-1}*Z_s'$ is applied at the X terminal, and Y at the Y terminal, the output of the divider is simply ε'. The resemblance of the Z curve in Fig. 2.14 and ε' curve in Fig. 2.10 is also due to this property. Using this property we will be able to measure ε' with the arrangement of Fig. 2.16. The details of the measurement will be reported in a later paper.

2.8. Conclusion af chapter 2

In this chapter, series solutions (for the case $Y=a+b\cos\omega t$) and operational solutions (for arbitrary waveforms) for the equation of motion of the analog divider are derived. With these two approaches, the dynamic characteristics of the divider are thoroughly studied. The results are summarized in the following.

(1) The division error ε can be divided into three components (ε_0, ε_k, ε_k') according to the origin of error being the loop gain characteristics, the dynamic characteristics of the multiplier or the multiplication effect of the above two. The component ε_0 is inherent to the feedback-type divider, and ε_k' is usually very small and hence is unimportant. The component ε_k becomes dominant when the dividend X has a strong spectrum outside of the practical frequency band of the multiplier. However, this as well as ε_k' can be eliminated by using a simple linear compensating element.

(2) According to the approximation solution (operational solution), the in-

stantaneous division error can easily be estimated from the magnitude of the divisor Y and the waveform (frequency spectrum) of the quasi-division error Z_s.

(3) The division error increases as (a) Y becomes small and (b) the frequency spectrum of Z_s' tends to distribute over the high-frequency region. Generally, because of the strong nonlinear relation between Y and Z_s', these two factors are equally influential.

(4) If the spectrum of Z_s' has large components in the vicinity of the frequency of the dominant characteristic roots of the feedback loop, there will be an oscillation (due to the dominant characteristic roots) in the divider output when Y is large.

(5) If the dividend input is Z_s' and the divisor input is Y, the output of the divider will be proportional to the quasi-division error $\varepsilon' = \varepsilon_0 + \varepsilon_k'$. This property is very useful in the measurement of division error.

3. Static Errors of Diode Quarter-Square Multipliers

3.1. Quarter-square multipliers and dividers based on linearly-segmented approximation

In Fig. 3.1, if the breakpoints are located at equal distances along the input axis and the slope of each segment is that of the parabola at the midpoint between breakpoints, it is possible that the output error is zero at two points in the intervals between breakpoints and has a negative value δ^- at the midpoint and equal positive values δ^+ at the end points.

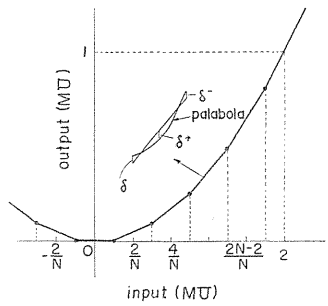

FIG. 3.1. Piecewise linear approximation to parabola.

Fig. 3.2 (a) shows a circuit that squares the sum of two inputs. In this circuit, by appropriate choice of the circuit constants, the diodes D_1, D_2, . . . successively conduct with the increase of $(u+v)$ and supply the current approximately proportional to $(u+v)^2$ to the summing junction of the output operational amplifier.

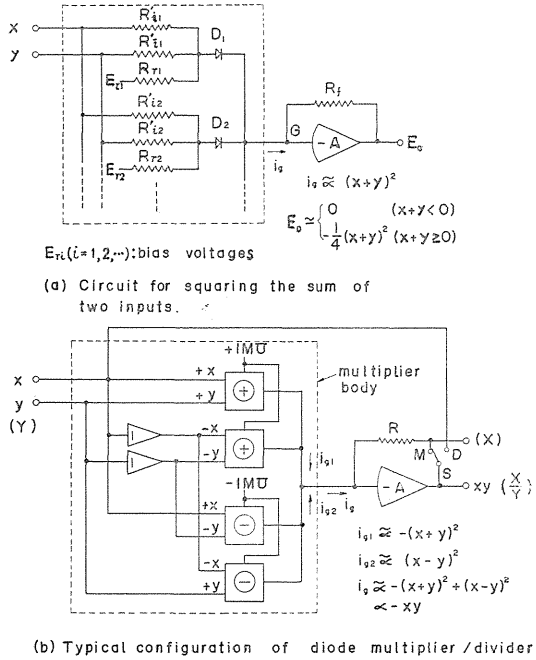

FIG. 3.2. Typical configuration of the biased-diode quarter square multiplier/divider.

A typical configuration of the multiplier or divider employing the squarer based on this principle is shown as Fig. 3.2 (b). The circuit bounded by the broken line may be regarded as an essential part or a body of the multiplier. Expressing this part by the ordinery multiplier symbol, Fig. 3.3 can be obtained as an equivalent circuit of the divider. Although the multiplier output is a current, for convinience we shall express the multiplier output by the voltage across the resistor R by this current. Fig. 3.2. (b) is so composed circuit that the total multiplier constant including the sign inversion by the output amplifier is positive, so that the multiplier constant of the multiplier body is negative. Thus the divisor Y in the divider case is restricted to the negative value.

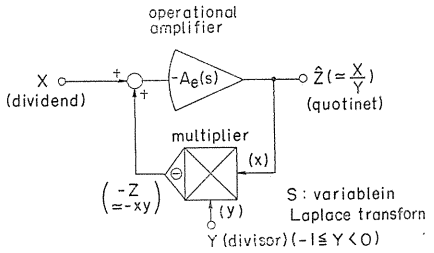

FIG. 3.3. Configuration of feedback-type divider (equivalent circuit).

3.2. Multiplication error

In the present and following sections, we assume that the squarer constructing the multiplier or divider has just as same characteristics as the piece-wise linear characteristics prescribed in Section 3.1. The effect of the deviation from this theoretical characteristics on squaring or multiplication error will be considered in later chapters.

The characteristics of a squarer which generates $(x+y)^2$ can be represented by a curved surface having a valley expressed by a straight-line $y=-x$ and a transverse section of a piece-wise linear curve of Fig. 3.1, as shown in Fig. 3.4 (a). Similarly the characteristics of the squarer for $(x-y)^2$ is shown in Fig. 3.4 (b).

These curved surfaces have creases parallel to the valley line $y=-x$, corresponsing to the segmented characteristics of Fig. 3.1. Now we define the per-quadrant segment number N by the number of the breakpoints included in posi-

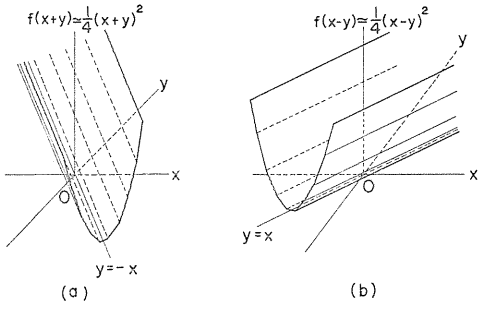

FIG. 3.4. Input vs. output characteristics of the two squarers constructing the multiplier.

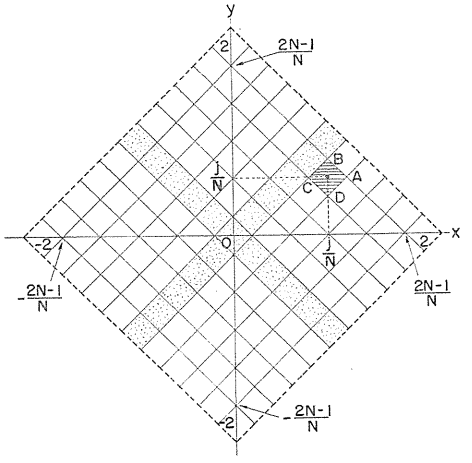

FIG. 3.5. Small square domains within which the multiplier operates as a linear element (I).

tive (or negative) input region in Fig. 3.1. A projection of the creases of the curved surface on the $x-y$ plane forms a family of straight lines, expressed by Eq. (3.1) or Fig. 3.5. Denoting by $(i/N, j/N)$ the co-ordinate of the center of a arbitrary small square domain formed by the straight-line family above, an equation giving its boudary line becomes

$$\left.\begin{aligned} y &= -x+\frac{i+j\pm 1}{N} \\ y &= x-\frac{i-j\pm 1}{N} \\ &\text{where } 0\leqq i,\ j\leqq N,\ i+j=\text{eve nnumber} \end{aligned}\right\} \tag{3.2}$$

If we difine the multiplier output z by the following equation:

$$x=f(x+y)-f(x-y) \tag{3.3}$$

then in a small square domain z can be expressed by a plane

$$z=\frac{j}{N}y+\frac{j}{N}x-\frac{ij}{N^2} \tag{3.4}$$

Then we find that Eq. (3.4) is a Tailor expansion of two variable function xy at the point $(i/N, j/N)$ where the second order term omitted (In this case the third or higher terms can not exist).

Next, defining a static multiplication error ε_m by the following equation:

$$\varepsilon_m=z-xy \tag{3.5}$$

from Eqs. (3.4) and (3.5) we obtain

$$\varepsilon_m(x, y)=-\left(x-\frac{i}{N}\right)\left(y-\frac{j}{N}\right) \tag{3.6}$$

Therefore the multiplier static characteristic is represented by many diamond-shaped facets on the skewed network formed by the intersections of the curved surface $z=xy$ (ideal multiplier characteristic) and a family of planes given by $x=i/N$, $y=j/N$ $(i=1, 2, \ldots N)$. Though Fig. 3.6 shows only one quadrant, the shapes of the curved surfaces $z=xy$ and $z=f(x+y)-f(x-y)$ in other quadrants can be easily understood from the property that they are odd-symmetrical with respect to x and y axises. From Fig. 3.6, the multiplier output characteristic curves expressed as a function of x with y as a parameter can be deduced (Fig. 3.7). Here the relation of input x to output z in the case of $j/N<y<(j+1)/N$ is given by a piece-wise linear curve in which the intervals of the slopes j/N and $(j+1)/N$ appear alternatively.

In Eq. (3.6), when $i=j=0$, we have $\varepsilon_m=-xy$. This forms a part of the negative ideal multiplication curved surface defined in small square domain with the diagonal lines on x and y axises. Refering Eq. (3.6), we know that the curved surface of ε_m in the whole domain can be obtained by arranging the just mentioned small curved surfaces according to the network shown in Fig. 3.5.

In Fig. 3.8 (a), ε_m takes the maximum value $1/(4N^2)$ at the center of an arc BC (or DA) and the minimum value $-1/(4N^2)$ at the center of an arc AB (or

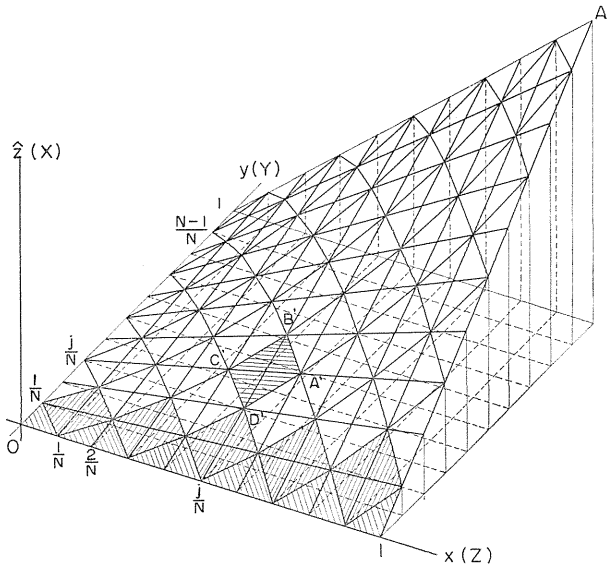

FIG. 3.6. Static characteristic of the diode multiplier (3-dimennsional representation).

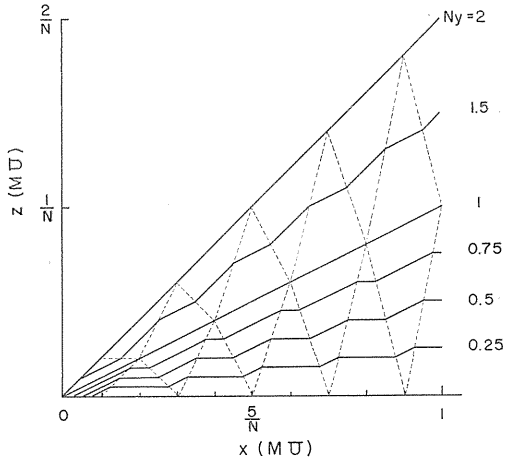

FIG. 3.7. Static characteristic of the diode multiplier (2-dimensional representation).

CD) and these values give a maximum error of the multiplier.

If we denote by $\varepsilon_M(y)$ the maximum multiplication error (absolute value) for $-1 \leqq x \leqq 1$ where y regarded as a parameter,

for
$$y = \frac{i}{N} + \frac{\delta}{N} \quad (0 \leq \delta \leq 1) \tag{3.7}$$

we have
$$\varepsilon_M(y) = \frac{1}{N^2}\delta(1-\delta) \tag{3.8}$$

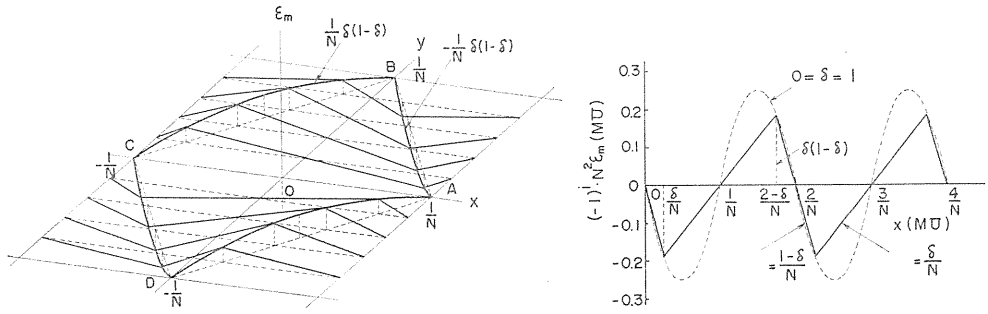

(a) Curved surface representing the static error. (b) Error curve with y as a parameter.

FIG. 3.8. Static errors of the diode multiplier.

Fig. 3.8 (b) shows the variation of ε_m obtained when x is swept from $0(MU)$ to $1(MU)$ for a fixed y, and the locus of each salient point of ε_m curve for the variation of δ is given by Eq. (3.8).

3.4. Error of dividers

As shown in Fig. 3.3, we have a divider by placing the multiplier in the negative feedback circuit of an operational amplifier. If we denote the dividend input, the divisor input and the quotient output by X, Y, and Z respectively, we obtain the following equations:

$$\left.\begin{aligned} y &= Y \\ z &= X \\ x &= Z \end{aligned}\right\} \tag{3.9}$$

where we assume that the amplification factor of the operational amplifier is sufficiently large.

Substituting Eq. (3.9) into Eq. (3.4), we have

$$Z = \frac{N}{j}X - \frac{i}{j}Y + \frac{i}{N} \tag{3.10}$$

where $0 \leq i,\ j \leq N$, $i+j$=even number.

The projection of each side of $\square A'B'C'D'$ on the $X-Y$ plane (or $z-y$ plane) is given by

$$\left.\begin{aligned} X &= \frac{i-j}{N}Y + \frac{j(j\pm 1)}{N^2} \\ X &= \frac{i+j}{N}Y - \frac{j(j\pm 1)}{N^2} \end{aligned}\right\} \tag{3.11}$$

In the small parallelogramic domains bounded by a set of four straight lines given by Eq. (3.11), the divider operates as a linear system. By Eq. (3.9), if z, y, and x axises are regarded as X, Y, and Z axises respectively, this figure transforms into a divider characteristic curved surface immediately*. Eq. (3.10)

* Though the graph obtained by the changes of variables lacks the domain for $Y<0$, from the symmetrical properties of the graph, we may discuss only the domain for $Y>0$ or regard X and Y axises as $-X$ and $-Y$ axises, respectively.

is shown by $\square A'B'C'D'$ in Fig. 3.6.

If we define the static error ε_d of the divider by

$$\varepsilon_d = Z - \frac{X}{Y} \tag{3.12}$$

we obtain

$$\varepsilon_d = \left(X - \frac{i}{N}Y\right)\left(\frac{N}{j} - \frac{1}{Y}\right) \tag{3.13}$$

Examining Eqs. (3.11) and (3.13), we see that ε_d is zero on the diagonal lines ($Y=j/N$ and $X=iY/N$) of $\square ABCD$ in Fig. 3.9 and that takes the maximum absolute value on the four sides corresponding to $Y=(1/N)\sqrt{j(j\pm1)}$.

Also, if we rewrite Eqs. (3.11) and (3.13) in the form of Eqs. (3.11′) and (3.13′):

$$\left.\begin{aligned} \frac{X}{Y} &= \frac{i-j}{N} + \frac{j(j\pm1)}{N^2Y} \\ \frac{X}{Y} &= \frac{i+j}{N} + \frac{j(j\pm1)}{N^2Y} \end{aligned}\right\} \tag{3.11′}$$

$$\varepsilon_d = \frac{N}{j}\left(\frac{X}{Y} - \frac{i}{N}\right)\left(Y - \frac{j}{N}\right) \tag{3.13′}$$

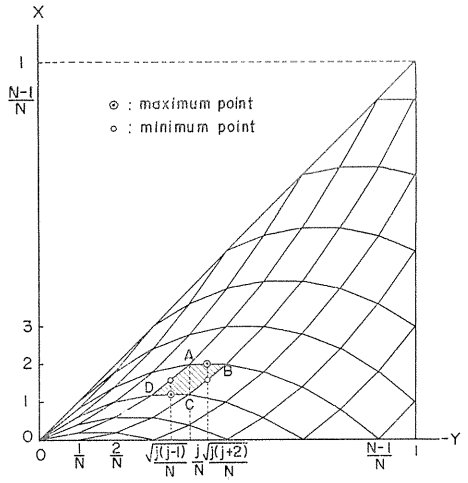

FIG. 3.9. Small parallelogramic domains within which the divider operates as a linear element (II).

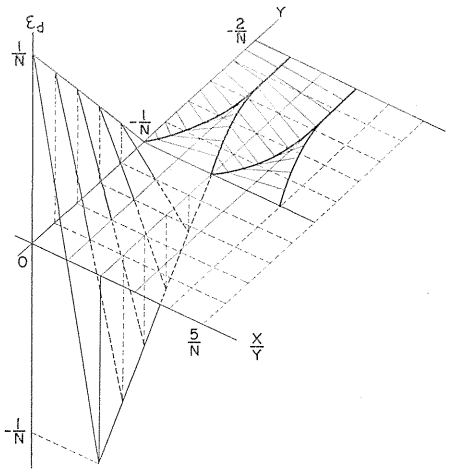

FIG. 3.10. Curved surface representing the static error of the divider.

the division error curved surface and the small parrallelogramic domains can be represented as in Fig. 3.10 and Fig. 3.11. Fig. 3.10 shows that the division error ε_d varies periodically with X/Y and that its maximum value ε_D is a function of Y.

For $-k/N \geq Y \geq -(k+1)/N$ (k is an integer satisfying $0 \leq k \leq N-1$), we have

$$\left.\begin{aligned} \varepsilon_D &= \frac{1}{N} + Y \qquad (k=0) \\ \varepsilon_D &= \frac{1}{Y}\left(Y+\frac{k}{N}\right)\left(Y+\frac{k+1}{N}\right) \qquad (k\leq 1) \end{aligned}\right\} \tag{3.14}$$

and, for $k\geq 1$, ε_D takes the maximum value

$$\varepsilon_{Dm} = \frac{1}{N}(\sqrt{k+1} - \sqrt{k})^2 \tag{3.15}$$

at

$$Y = -\sqrt{k(k+1)}/N \equiv Y_k \tag{3.16}$$

This situation is illustrated by Fig. 3.11 and Fig. 3.12.

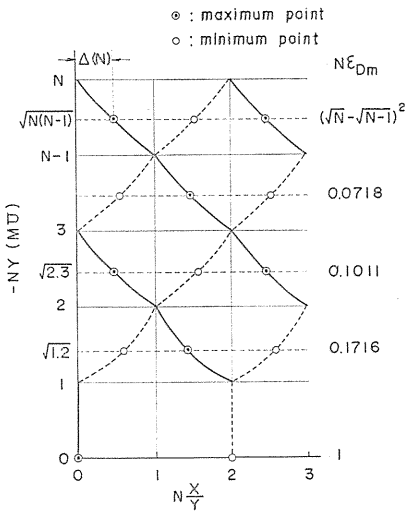

FIG. 3.11. Small domains within which the divider operates as a linear element.

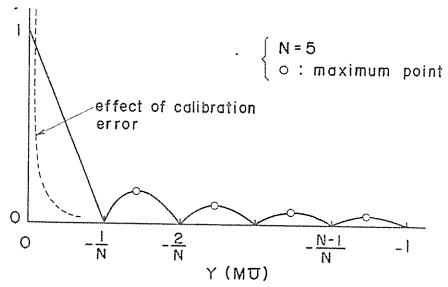

FIG. 3.12. Relation between the divisor input Y and the maximum (static) division error.

As Fig. 3.10 shows, the division error is particularly large for $-(1/N)\leq Y\leq 0$ (maximum value is $1/N$ in this region) and the division error curved surface is discontinuous at $X/Y=2k/N$ (k: integer). This qualitatively explains the jumping phenomena of the divider output and the increase of the output noise observed when $|Y|$ is small. On the other hand, if Y increases, tending to -1, we have

$$\varepsilon_{Dm} = \frac{(\sqrt{N}-\sqrt{N-1})^2}{N} = \left(1-\sqrt{1-\frac{1}{N}}\right)^2 \simeq \frac{1}{4N^2} \tag{3.17}$$

and ε_{Dm} becomes approximately equal to the maximum multiplication error.

Moreover, in order to improve the small input multiplication characteristic, sometimes the breakpoints of the squarer characteristic are closely located near the origin. However, as this effect appears only in and near the dotted domain

in Fig. 3.5, this has no effect on the improvement of the division accuracy.

3.4. Effect of calibration error

Diode squarers or multipliers cannot be produced and calibrated perfectly in every case, and changes in temperature and circuit constants variations with time can produce additional errors.

Since the causes of these additional errors are attributable to the variations of the breakpoint positions and segments slopes of the approximation curve to parabola, we can discuss, without loss of generality, only the calibration error. The basic (broken line) characteristic composing the piecewise-linear approximation curve to parabola is shown by a solid line in Fig. 3.13 (a). If its breakpoint is shifted as shown in a broken line A or B, the squarer produces the error denoted by A or B respectively. Therefore the errors of two squarers are represented, for example, by (b) and (c) in the same figure. The zero error of the multiplier $\varepsilon_m(x, 0)=\varepsilon_{mc}(x, 0)$, where $\varepsilon_{mc}(x, y)$ represents the calibration error of the multiplier, is given by $\varepsilon^+-\varepsilon^-$ shown in (d).

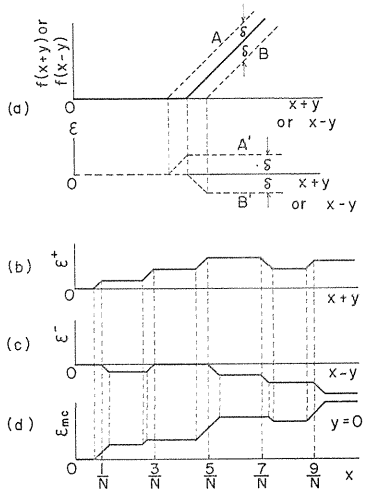

FIG. 3.13. Multiplication error based on the calibration errors of the squarers.

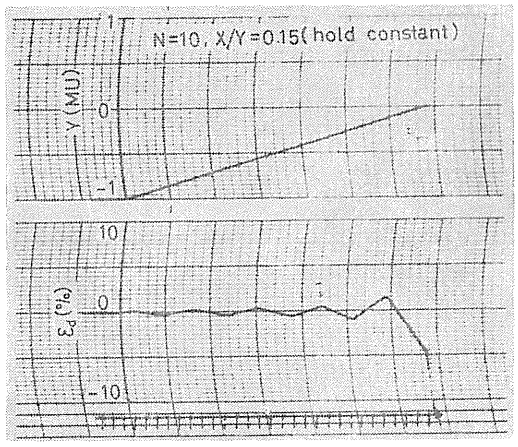

FIG. 3.14. Example of the division error (measured).

As seen from the divider characteristic in Fig. 3.14, we can relate a maximum divider error $\varepsilon_D(Y)$ in the range $-1\leq X\leq 1$ where Y fixed, to the maximum multiplication error $\varepsilon_M(Y)$ in the range $-1\leq x\leq 1$ where $Y(=y)$ fixed. That is,

$$\varepsilon_D(Y)=\varepsilon_M(Y)/Y \tag{3.18}$$

In the case of no calibration error, since $\varepsilon_M(Y)\to 0$ as $Y\to 0$, as seen from the discussion in Section 3.4, $\varepsilon_D(Y)$ tends to a finite value $1/N$; otherwise, as $\varepsilon_M(Y)$ approaches to a finite value given by Fig. 3.13 (d), for $Y\to 0$, $\varepsilon_D(Y)$ rapidly increases to infinity as $Y\to 0$. This effect is qualitatively illustrated by a broken line in Fig. 3.12. Fig. 3.14 is a record of the division error measurement where the multiplier with $N=10$ was used and Y swept $-1(MU)$ to $0(MU)$ keeping

$X/Y=0.15$. This proves the characteristic figure shown in Fig. 3.10. The scaling out of the divider output just before Y reaches zero suggests the calibration error effect discussed above. Although this error can be analysed in more detail by the use of Fig. 3.6, we shall not discuss further in this paper.

Now, if two squarers have no ideal characteristics while the two characteristics are equal, no effect of calibration error appears in the small square domains including X axis as diagonals. Although in the small squares adjacent to the above the multiplication error appears, it can not exceed an error δ of each basic characteristic of the squarers. Because its value is generally small, only if we have a good agreement between the positive input characteristics of two squarers ($\varepsilon_m(x,0)\simeq 0 (x>0)$), even if neither has the ideal characteristic, a considerable reduction in division error originated from calibration error may be expected.

3.5. Effects of the forward characteristics of diodes

Actual diode characteristic shown in Fig. 3.15 smoothes the linear segmented characteristic in Fig. 3.1 and thus every graph derived from this have corners or creases smoothed. As a result, the maximum of the actual multiplication error only by the piecewise-linear approximation is smaller than the theoretical value obtained in Section 3.3. Apparently this effect becomes remarkable as N increases. Fig. 3.16 is a comparison between that maximum multiplication errors by piecewise linear approximation which are found in comercially available diode multipliers and the corresponding theoretical values. As seen from Fig. 3.16, the theoretical values varies inversely as N^2 while the actual values as $N^{2.52}$. However, the reduction of the multiplication error due to the diode characteristic is canceled out by the calibration error of actual multiplier and $1/(4N^2)$ seems to serve as a standard of the practical maximum multiplication error due to the piecewise linear approximation alone.

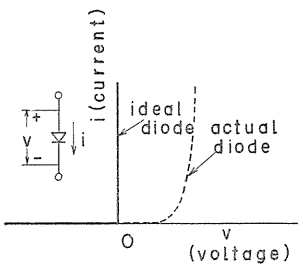

FIG. 3.15. Voltage-current characteristic of diode.

On account of limited space, important methods and results are discribed concisely and full discussion will be published anywhere.

3.5.1. Design theory

From Fig. 3.2 we can write the static equivalent circuit of diode squarer as in Fig. 3.17. Here f_{ks} in (a) denote input-output characteristic of the circuits in (b).

As is well known, the theoretical voltage-current characteristic of semiconducter diodes is represented by

$$I=I_0(e^{\frac{V}{\lambda V_T}}-1) \tag{3.20}$$

where $V_T=0.026\,(V)$ at 302° K.
Usually for the silicon diode λ is taken as 2.

In Fig. 3.17, recognizing that the summing point voltage of operational amplifier is held zero, we can obtain the relation between E_{iok} and input current I by using Eq. (3.20).

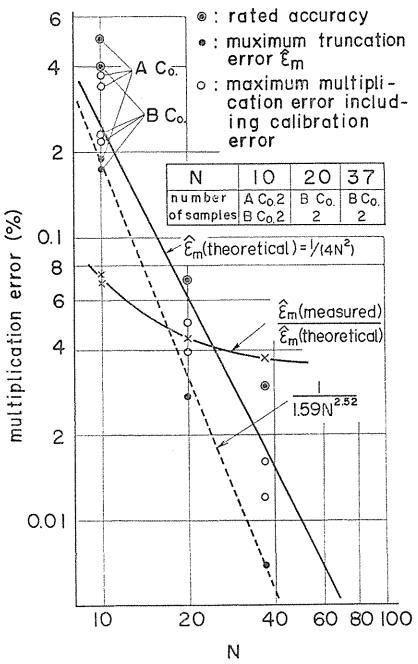

FIG. 3.16. Examples of errors found in commercial diode multipliers.

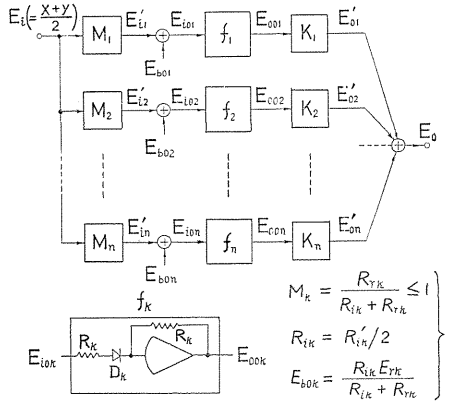

FIG. 3.17. Equivalent circuit of diode multiplier.

Since the input current flows through the feedback resistor R_k, E_{ook} becomes equal to $-R_k$ times the input current and hence the following equation results.

$$E_{io} = E_{oo} + V_T \log e \left(1 + \frac{E_{oo}}{RI_o}\right) \tag{3.21}$$

Here the subscripts are dropped for favor of simplicity.

Eq. (3.21) shows that the E_{io} vs. E_{oo} relation is determined by the product RI_o rather than by R or I_o individually.

In Fig. 3.18 E_{oo} is plotted as a function E_{io} with RI_o as a parameter, where the values of E_{oo} for given E_{io} were computed by applying Newton-Raphson method to Eq. (3.21). If we denote by $E_{oo}=f(E_{io}, RI_o)$ the functional relation between E_{io} and E_{oo} for an arbitrary value of RI_o, then a curve for another value $(RI_o)'$ of RI'_o namely $E_{oo}=f\{E'_{io}, (RI_o)'\}$ coincides at infinity ($E_{iok}=\infty$) with the graph of $E_{oo}=f(E_{io}, RI_o)$ moved parallel to the left by $\lambda\ V_T \cdot \log_e\{(RI_o)'/(RI_o)\}$. In Fig. 3.19, the difference between them for finite values of E_{io} is shown for different values of RI_o. Actually the value of RI_o may vary with every segment and every specification. If there is 1 : 100 difference between the values of RI', for example, $10^{-5}(V)$ and $10^{-3}(V)$, then the maximum difference between the two (after moving paralell) is about 1 (mV). This value is not necessarily small enough in comparison with the maximum errors of practical squarers. However, in a squarer with a rated maximum error 2 (mV), for example, the values of K'_ks are of the order of 10^{-1} as will be clear later, and hence 1 (mV) is multiplied by about 10^{-1} and the difference appeared in the output much smaller than 2

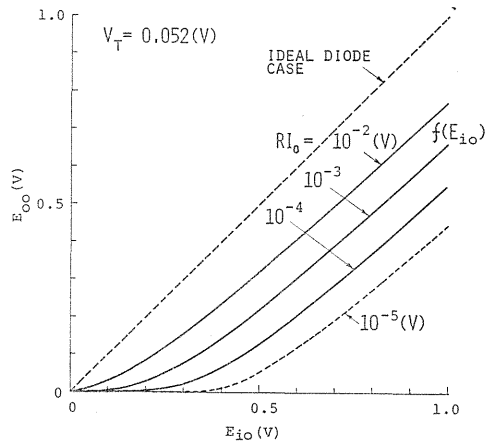

FIG. 3.18. E_{oo} as a function E_{io} with RI_o as a parameter.

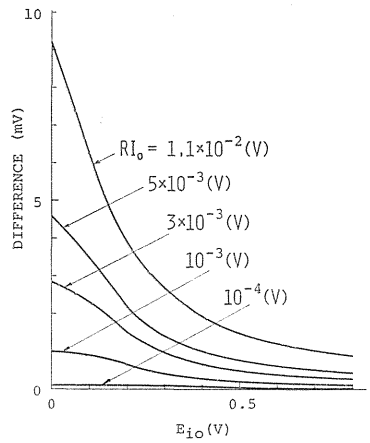

FIG. 3.19. Fitting between the functions having different values of R_o.

(mV). Although general discussion is omitted here, for most cases the above holds true.

Now we may say that a variation of RI_o is equivalent to a shift of the "effective breakpoint". Consequently we may treat only the curve for the most probable value of RI_o $(=10^{-4}(V))$. If a value of RI_o differs from this specified value $10^{-4}(V)$, the designer need only to choose E'_{iok} lower by $\lambda V_T \log(10^{-4}/RI_o)$. First, if we assume $M_1=M_2=\cdots=M_n=M=1$, then from Fig. 3.16 and the above discussion the output E_o of squarer can be written as

$$\left.\begin{aligned} E_0 &= \sum_{k=1}^{n} E'_{ok} = \sum_{k=1}^{n} K_k f_k(E_i - E_{bok}) \simeq \sum_{k=1}^{n} K_k f(E_i - E'_{bok}) \\ \text{where } E_{bok} &= E'_{bok} + \lambda V_T \log_e\{(R_k I_{ok})/(RI_o)\} \end{aligned}\right\} \tag{3.22}$$

Therefore the design problem is reduced to a problem: Find the values of $K'_k s$ and $E'_{bok} s$ such that a specified maximum error rating is satisfied with minimum number of segments.

The solution of this problem was performed by a small digital computer (FACOM 270-10) under a close man-machine communication.

The values of E'_{bok} and K_k obtained in this way are shown in Fig. 3.20; it should be noted that the relation of E'_{bok} to segment number or interval number k is linear; that is, the breakpoints E'_{bok} are equally spaced; and therefore we can represent these intervals by one quantity Δ and we shall call it an inner interval of the squarer. In Fig. 3.21, (1) the maximum error ε of the squarer (where the subscript of ε indicates a voltage E_m corresponding to a machine unit.), (2) the numbers $\hat{N}$ and $\tilde{N}$ of segments required for the squarer when the diodes have the ideal characteristic and exponential one $(\lambda=2)$, and (3) the error reduction factor $F_R=|\varepsilon|_{\max}/|\hat{\varepsilon}|_{\max}$, are plotted as functions of Δ.

(a) The maximum output temperature coefficient F_T

In semiconductor diodes, whether germanium or silicon, the voltage across

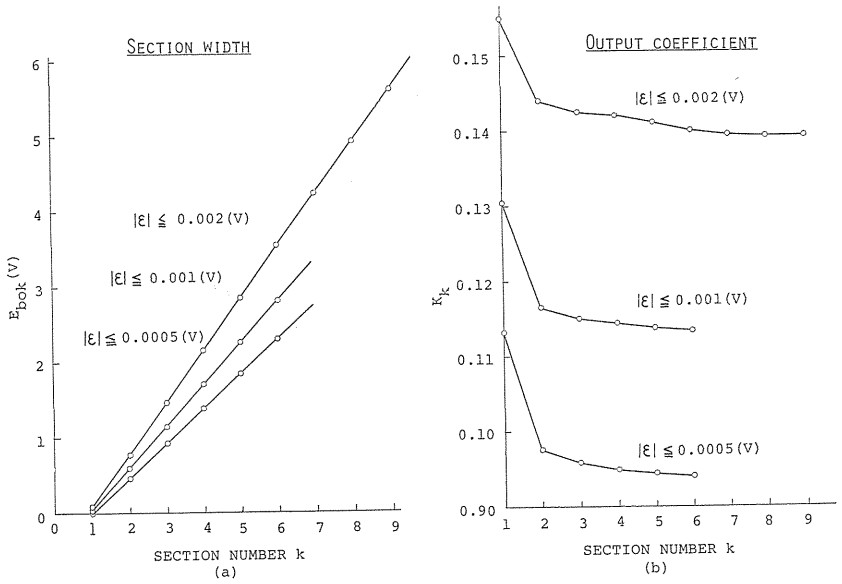

FIG. 3.20. Values of E_{iok} and K_k ($k=1, 2, 3, \ldots$).

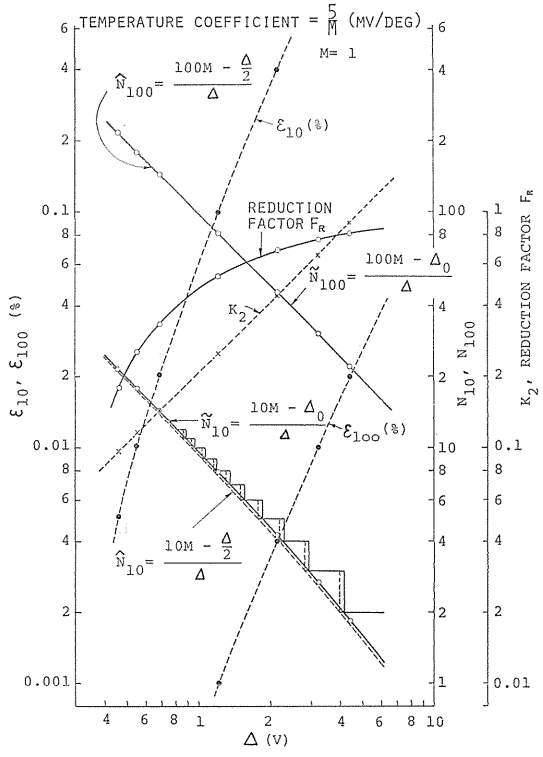

FIG. 3.21. Concentrated data for designing the diode multiplier.

the diode for a given constant current decreases by about 2.5 mV for each one degree centigrade temperature increment. If we assume the temperature coefficient of -2.5 mV/°C, the increase (in percentage for a machine unit) F_T of squarer output with temperature is given by

$$F_T = \frac{0.5}{(E_{io})_{\max}} (\%/°C) \tag{3.23}$$

where $(E_{io})_{\max} = \Delta_o + \tilde{N}\Delta$,
where Δ_o denote a distance from the origin to the first effective breakpoint.

Therefore, for a fixed N, decreasing F_T leads to increasing Δ; however, increasing Δ conflicts with the condition for decreasing F_R as seen from Fis. 3.21. Therefore, an allotment between F_R and F_T should be determined according to the practical use of the multiplier, or by the design policy.

Since $M_k \leq 1 (k=1, 2, \ldots, n)$ and thus $(E_{io})_{\max} \leq E_m$ and $E_T \leq \frac{0.5}{E_m}$, the freedom of design increases with E_m.

(b) Case when $M_1 = M_2 = \cdots = M_n = M < 1$

In this case we have

$$E_{io} = ME_i \tag{3.24}$$

so that

$$(E_{io})_{\max} = M(E_i)_{\max} = ME_m = \Delta_o + \tilde{N}\Delta \tag{3.25}$$

Hence, for a fixed value of Δ, if we neglect Δ_o, N decreases proportionately as M is decreased. However, since the output coefficients K_k then must be multiplied by $(1/M^2)$ in order to obtain the same output level, the maximum error also is multiplied by $(1/M^2)$ and thus increased in proportion to $(1/\tilde{N}^2)$. That is, we see that the variation of the maximum error against the required number $\tilde{N}$ of segments follows the theoretical law $1/4N^2$ given previously.

When not all of M_k are equal, the design becomes rather complex, although interesting, and this case is omitted in this paper.

(c) Actual values of λ

In order to know actual values of λ, the voltage-current relation of the series combination circuit of diode and resistor was measured for commercially available silicone diodes suitable for this pourpose (1 S 1220 and 1 S 1219). In experiment we used a matal film resistor having 0.5% accuracy and 25 ppm/°C temperature coefficient; the circuit was placed in a thermobox set for (23 ± 0.1)°C; voltages were applied to this circuit by a standard voltage generator having 0.1% accuracy and less than 10 μV output drift, and voltages accross the resistor instead of currents through it were measured by a digital voltmeter with 0.1% accuracy.

TABLE 3.1. Experimental values of λ and I_0

diode	number of samples	λ	I_0
1 s 1219	15	1.997 ± 0.055	4.6–7.8 (nA)
1 s 1220	13	2.015 ± 0.052	5.1–7.85 (nA)

Data from this procedure were processed by a small digital computer, the values of λ and I_o being obtained. The results are summarized in Table 3.1; we see that λ is very exactly equal to 2; in contrast, a scattering of the values of I_o is noticed, but this is unimportant for the reason mentioned above.

3.7. Conclusion of chapter 3

(1) The theoretical maximum multiplication error based on the truncation error in ideal diode case is $1/(4N^2)$ where N denotes the number of breakpoints per quadrant. However, because of the diode characteristic, the actual maximum multiplication error, not including calibration error, obeys a empirical formula $1/(1.59N^{2.52})(\%)$.

(2) The maximum division error in the range $-1\leq X\leq 1$ is determined by the magnitude of divisor input Y; generally the division error can go over the maximum multiplication error and is below this or so when $|Y|$ approaches $1(MU)$. In particular, when $0\leq|Y|<1/N$, the division error can increase in amplitude; the divider output characteristic is discontinuous on straight line segments $X/Y=2k/N$ (k: integer) and hence the point $(X/Y, Y)$ crosses any line of discontinuity the divider output changes by $2\{(1/N)+Y\}(MU)$ discontinuously. When $|Y|$ is very close to zero, then the calibration error effect is remarkable. Then an output jump larger than the above theoretival value occurs and the division error can become much larger than the theoretical maximum division error $1/N$ in the whole operating domain.

(3) If the characteristics of the two squarers are equal, even if each square has a calibration error, an remarkable increase in division error due to calibration error can be avoided. The identity between the characteristics of the two squarers can easily be checked by measuring the zero error ($0\leq x\leq 1$) of multiplier for $y=0$.

(4) For example, in the case of the commercial triangularwave multiplier with 0.2% half scale accuracy, the division error is 1–2% when divisor $=0.01$ (MU); however the diode multiplier with the same rated accuracy has N less than 15 as can be read off from Fig. 3.16 and hence from Fig. 3.12 the truncation division error is found to be 5.67% when the divisor $=0.01$ (MU).

Since the error reduction due to the diode-characteristic usually tend to be canceled out by the calibration error, we may say that an increase in operational error experienced when changed into the divider configuration, is more remarkable in the diode multiplier.

(5) The error reduction factor F_R of squarer due to the actual diode-characteristic is determined by the inner interval Δ regardress of the maximum operating voltage E_m. Although for a given $\tilde{N}$ the maximum multiplication error decreases as Δ becomes small, the temperature coefficient F_T of the multiplier output increases nearly inversely as Δ is decreased. In short, the design of diode squarers or multipliers is reduced to a proper choice of Δ. The range of allowable values of Δ widens as E_m is increased.

4. Several Problems Pertaining to the Computer Circuit Including Multipliers or Dividers

As a continuation of the characteristic analysis of the multiplier or divider itself, this chapter is devoted to solve the many problems which occur when

multipliers or dividers are contained in analog computer circuits of differential equations.

4.1. Effects of the truncation error on the solution of the equation of simple harmonic motion

In this section, we shall investigate the effects of the multiplier or divider error on the computer solution by inserting diode multiplier with one input constant or a divider derived from this multiplier with a divisor input constant into the so-called circle test circuit, as shown in Fig. 4.1. The diode multiplier or divider, even if the input is sinusoidal, generally produces higher harmonics because of its trncation error. Since there are two integrators in the loop of the circle test circuit, we may expect sufficient attenuations of higher harmonics round the loop and shall attempt to express the characteristic of the multiplier or divider with one input constant by a describing function.

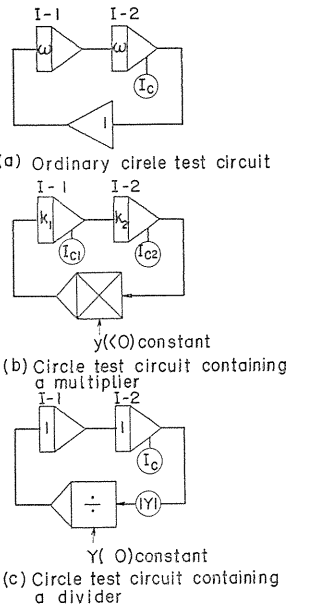

FIG. 4.1. Various circle test circuits.

4.1.1. Case of the multiplier

From the results of the analysis given in Section 3.3, the multiplier characteristic, regarding Y as a parameter, is illustrated in Fig. 4.2, where $f_N(x, y)$ denotes the output of the multiplier with N segments per quadrant, $\left[\frac{j}{2}\right]$ Gaussian symbol, and a, b, c, d which give the co-ordinates of the breakpoints are determined by Eq. (4.1).

$$\left.\begin{aligned} a &= \frac{1}{N} - Y \\ b &= 2y \\ c &= \frac{2a}{N}\left[\frac{j}{2}\right] = \frac{2}{N}\left(\frac{1}{N} - y\right)\left[\frac{j}{2}\right] \\ d &= \frac{2b}{N}\left\{\left[\frac{j}{2}\right] + \frac{1}{2}(-1)^{j-1}\right\} = \frac{4y}{N}\left\{\left[\frac{j}{2}\right] + \frac{1}{2}(-1)^{j-1}\right\} \end{aligned}\right\} \tag{4.1}$$

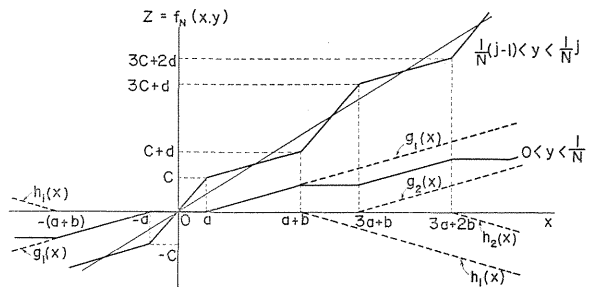

FIG. 4.2. Static characteristic of the diode multiplier (general representation).

Now, for $0<y_1<1/N$, we define y_j as

$$y_j = y_1 + \frac{j-1}{N} \quad (j=1, 2, 3, \ldots) \tag{4.2}$$

Then the multiplier input (x) vs. output characteristic $f_N(x, y)$ can be expressed by

$$\begin{aligned} &f_N(x, y_j) = \frac{2}{N}\left[\frac{j}{2}\right]x + (-1)^{j-1} f_N(x, y_1) \\ &\frac{1}{N}(j-1) < y_j < \frac{1}{N}j \end{aligned} \tag{4.3}$$

Assuming that $x=\xi\cos\omega t$ $(\xi\geq 0)$, the describing function[22] $D_N(\xi, y_j)$ associated with $f_N(x, y_j)$ is given by

$$D_N(\xi, y_j) = \frac{1}{\pi\xi}\int_0^{2\pi} \{f_N(\xi\cos\omega t, y_j)\cdot\cos\omega t\} d(\omega t) \tag{4.4}$$

Accordingly the describing functions of Eq. (4.3) become

$$D_N(\xi, y_j) = \frac{2}{N}\left[\frac{j}{2}\right] + (-1)^{j-1} D_N(\xi, y_1) \tag{4.5}$$

and thus we need to investigate $D_N(\xi, y)$ only for $0<Y<1/N$.

Then, $f_N(x, y_1)$ for $y=y_1$ can be decomposed to the functions expressing dead zone characteristics $g_i(x)$ and $k_i(x)$ given by Fig. 4.2 or Eq. (4.6).

$$\left.\begin{aligned} f_N(x, y) &= \sum_j g_i(x) + \sum_j h_i(x) \\ g_i(x) &= \begin{cases} 0 & [|x| \leq (2i-1)a + (i-)b] \\ \frac{1}{N}\{x - (2i-1)a - (i-1)b\} & [x > (2i-1)a + (i-1)b] \\ \frac{1}{N}\{x + (2i-1)a + (i-1)b\} & [x < -(2i-1)a - (i-1)b] \end{cases} \\ h_i(x) &= \begin{cases} 0 & [|x| \leq (2j-1)a + jb] \\ \frac{1}{N}\{x - (2j-1)a - jb\} & [x > (2j-1)a + jb] \\ \frac{1}{N}\{x + (2j-1)a + jb\} & [x < -(2j-1)a - jb] \end{cases} \end{aligned}\right\} \tag{4.6}$$

Therefore the describing function $D_N(\xi, y_1)$ can be expressed in the sum of those of $g_i(x)$ and $h_i(x)$ as in Eq. (4.7).

$$\begin{aligned} D_N(\xi, y) = &\frac{1}{\pi N}\sum_{i=1}^{\left[\frac{\xi+a+b}{2a+b}\right]} (\cos^{-1}\alpha_i - \alpha_i\sqrt{1-\alpha_i^2}) \\ &- \frac{1}{\pi N}\sum_{j=1}^{\left[\frac{\xi+a}{2a+b}\right]} (\cos^{-1}\beta_i - \beta_i\sqrt{1-\beta_i^2}) \end{aligned} \tag{4.7}$$

where

$$\alpha_i = \frac{(2i-1)a+(i-1)b}{\xi} = \beta_i - \frac{b}{\xi}$$
$$\beta_j = \frac{(2j-1)a+jb}{\xi} \tag{4.7}$$

In Fig. 4.1 (b), if we choose the integrator constants k_1 and k_2 so that the angular frequency of the solution may be 1 rad/sec when the multiplier has the ideal characteristic, then the actual loop gain $G_N(\xi, y_j)$ at 1 rad/sec is

$$\left.\begin{aligned} G_N(\xi, y_j) &= \frac{D_N(\xi, y_j)}{y_j} \\ &= \frac{\frac{2}{N}\left[\frac{j}{2}\right]+(-1)^{j-1}\cdot D_N(\xi, y)}{\frac{j-1}{N}+y_1} \equiv 1+\varepsilon_N(\xi, y_j) \end{aligned}\right\} \tag{4.8}$$

Accordingly the period T (sec) of the solution becomes

$$T = 2\pi/\sqrt{G_N(\xi, y_j)} \tag{4.9}$$

Since Eq. (4.8) is written as

$$G_N(\xi, y_j) = \frac{\frac{2}{N}\left[\frac{j}{2}\right]+(-1)^{j-1}\cdot y_1 G_N(\xi, y_1)}{y_1+\frac{j-1}{N}} \tag{4,10}$$

we have

$$\varepsilon_N(\xi, y_j) = \frac{\{(-1)^{j-1}-1\}\left(y_1-\frac{1}{2N}\right)}{y_1+\frac{j-1}{N}} + \frac{(-1)^{j-1}\cdot y_1}{y_1+\frac{j-1}{N}}\cdot\varepsilon_N(\xi, y_1) \tag{4.11}$$

Thus the period decerases as j is increased. Then apparently

$$\lim_{N\to\infty}\varepsilon_N(\xi, y_j) = 0 \tag{4.12}$$

Fig. 4.3 shows relative errors of the solution period T computed by Eqs. (4.7)-(4.9) to the true value 2. Fig. 4.4 is a comparison of the calculated results with experimental results. Here "cos" represents the case where the initial value are given the integrator 2 and "sin" the case where the integrator 1 is given such an initial value that, if the solution is exactly sinusoidal, the amplitude of the solution becomes equal to that in "cos" case. In the case of "cos", although there is some discrepancy in the average periode between the calculated and measured values, an essential agreement is obtained in the manner of variation with solution amplitude. Accordingly we might consider the describing-function method to be sufficiently accurate to interpret the period error of solution. The

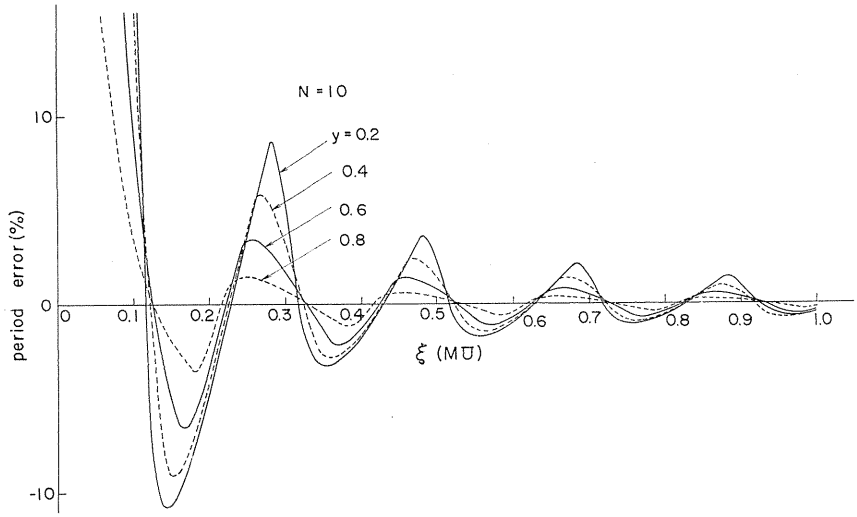

FIG. 4.3. Relation between the solution amplitide ξ and the solution period error (determined by describing-function method).

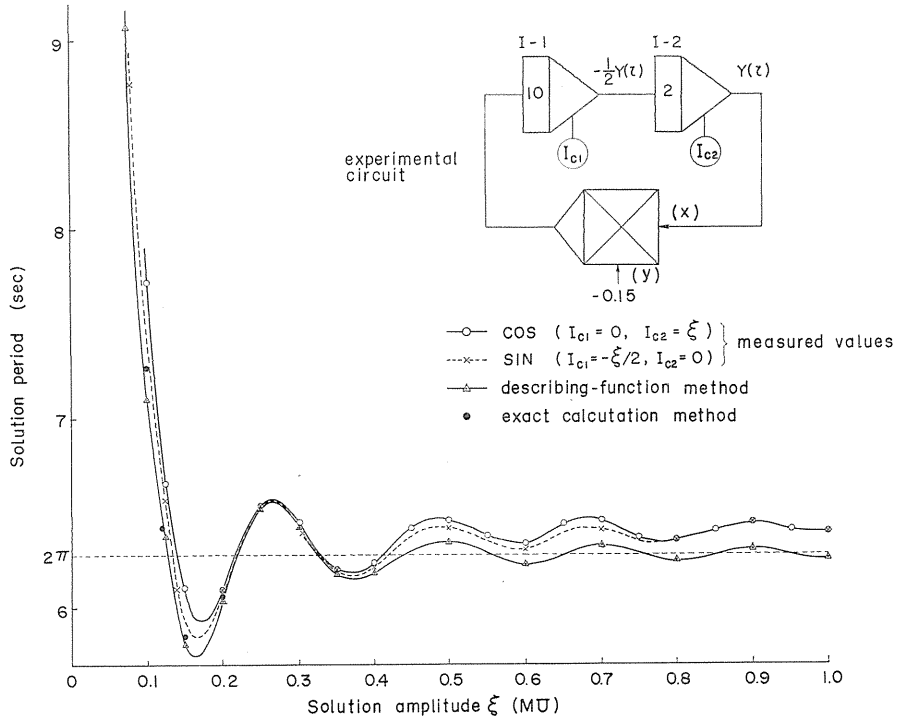

FIG. 4.4. Relation between the solution amplitude and the solution period in the circle test circuit containing the diode multiplier ($Y = -0.05$)

origin of discrepancy between the calculated and measured values may be considered to be the approximation inherrent to the describing function method and also the calibration error of the actual multiplier. In the case of "sin", however, the measured values are rather different even from the values by an exact calculation method and hence we may regard the effect of the calibration error to be rather notable.

As seen from Fig. 4.3 and Fig. 4.4, in the range of small amplitudes, the solution period makes a remarkable and oscillatory variation with solution amplitude. The approximate values (calculated) of amplitudes such that the periode error is zero, are 0.124, 0.225, 0.326, 0.427, ..., when $y=-0.05$. These values are fairly different from the values such that the average value of the deviations from the ideal curve over the dynamic range of y vanishes. Furthermore, the period error $\varepsilon_T(\xi, y)$ in Fig. 4.3 can be approximated in a relative error within a few percents by the following:

$$\varepsilon_T(\xi) \simeq \xi^{-1.5} \cdot f(\xi, Y) \tag{4.13}$$

where $f(\xi, y)$ is a oscillatory function having the periode of 0.2. Therefore the maximum period error of the solution is inversely proportional to $\xi^{3/2}$ or $N^{3/2}$.

Moreover the period error for $1/N \leq y \leq 1$ can easily be estimated from the equations such as Eq. (4.10).

4.1.2. Case of the divider

If we denote the inputs-output characteristic by $Z=F_N(X, Y)$, the relation between X and $F_N(X, Y)$ with Y as a parameter is obtained by the exchange of the ordinate and abscissa in Fig. 4.2, of which procedure is based on Eq. (3.9). A case for $-1/N<Y<0$ is shown in Fig. 4.5. Decomposing this into a linear characteristic and many relay element characteristics generally having deadzone, and summing the describing functions for them lead to the describing function $D_N(\xi, Y)$ of the divider. That is,

$$D_N(\xi, Y) = N + \frac{4a}{\pi\xi} \sum_{i=1}^{[\xi/b]} \sqrt{1-\left(\frac{ib}{\xi}\right)^2} \qquad (-1/N<Y<0) \tag{4.14}$$

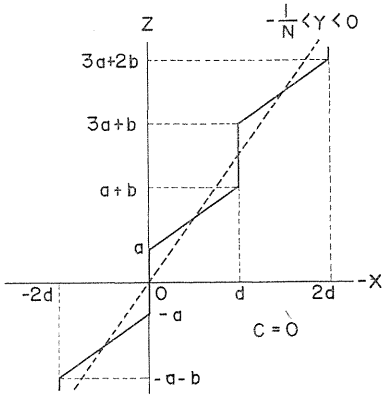

FIG. 4.5. Relation between the input X and the output of the divider for $-1/N<Y<0$.

An experiment for this case was made in a circuit of Fig. 4.1 (c). If the divider has the ideal characteristic, then the solution period should be 2 (rad/sec) regardless of the value of Y. A loop gain $G_N(\xi, Y)$ of this circuit at 1 (rad/sec) is

$$G_N(\xi, Y) = |Y| \cdot D_N(\xi, Y) \qquad (-1/N<Y<0) \tag{4.15}$$

and the solution period T can be obtained from Eq. (4.9).

The period error for $-1 \leq Y \leq -1/N$ can be computed by the method similar to that of the multiplier case. As in the multiplier, the period decreases with oscillation as $|Y|$ is increased.

Fig. 4.6 is a comparison between the theoretical values and the measured values for the case of $Y=-1/(2N)=-0.05$ $(N=10)$. The theoretical curve has cusps at $\xi=0.2$, 0.4, 0.6, 0.8 and these cusps correspond to the discontinuity points of the divider input-output characteristic $F_N(\xi, Y)(-1/N \leq Y<0)$. Although there is some discrepancy between the averages of the theoretical and measured values, their manners of variation with ξ are similar. The broken line in the same figure shows the measured values in the case of $Y=-0.5$; as in the multiplier the considerable reduction of the period error can be observed.

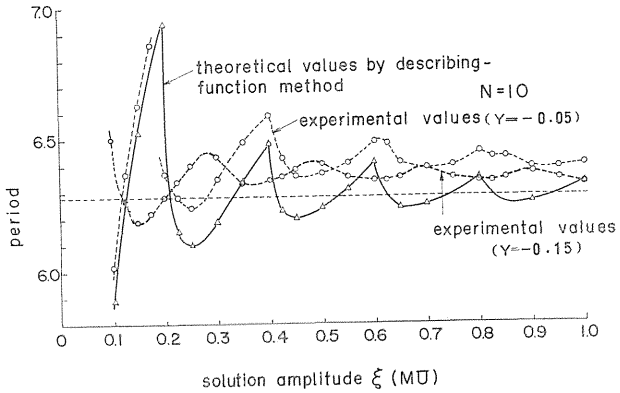

FIG. 4.6. Relation between the amplitude and the period of the solution in the circle test circuit containing the divider.

4.2. Case of Mathieu equation

Mathieu equation given by Eq. (4.16) is possibly the most important and simple one in the equations which require one or more multipliers for their solution.

$$\frac{d^2y}{dz^2}+(a-2q\cos 2z)y=0 \tag{4.16}$$

where a, q are constants.

To solve this by analog computer, we denote the scale factors of y, z by a_y, a_t respectively and transform Eq. (4.16) into Eq. (4.17).

An analog computer cercuit for Eq. (4.17) is given, for example, by Fig. 4.7. Since, for a certain choice of the values of a and q, operational errors of linear computing elements may affect the computer solution to a considerable degree, then an experiment by the analog computer cannot be fully successful for the investigation of the computer solution error due only to the truncation error. As a solution to this problem, a digital computer simulation for the circuit of Fig. 4.7 was performed on the basis of the analysis of Chapter 3.

4.2.1. Digital computer simulation of the analog computer circuit

After this, we shall append a number m to the line segment for the interval

$[(2m-1)/N,\ (2m+1)/N]$ of the squarer characteristic and call a small square formed by m and n segments of two squarers, which produce $(x+y)^2$ and $(x-y)^2$ respectively, a (m, n) domain. The relation of m and n to i and j is given by

$$\left.\begin{aligned} &m=\frac{i+j}{2},\quad n=\frac{i-j}{2} \\ &\text{or } i=m+n,\ j=m-n \end{aligned}\right\} \tag{4.18}$$

Now we rewrite Eq. (4.18) as

$$\frac{d^2Y}{d\tau^2}+PY+\frac{Q}{0.95}\left(\cos\frac{2}{a_t}\right)\cdot(0.95\,Y)=0 \tag{4.17'}$$

and, noticing that

$$\left.\begin{aligned} &x=0.95\,Y \\ &y=\cos\frac{2}{a_t} \end{aligned}\right\} \tag{4.19}$$

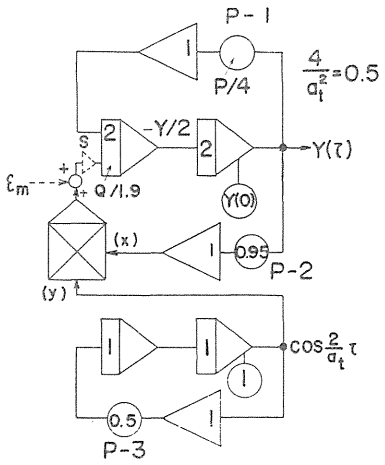

FIG. 4.7. Analog computer circuit for Mathieu equation.

we expand the third term of the left hand side of Eq. (4.17') by Eq. (3.4), where we assume that the point (x, y) is in (m, n) domain. Then we obtain constant coefficient linear equations (4.20) having a forcing term.

$$\left.\begin{aligned} &\frac{d^2Y}{d\tau^2}+FY=\frac{Q}{0.95}\cdot\frac{ij}{N}-\frac{Q}{0.95}\cdot\frac{i}{N}\cos\frac{2}{a_t}\tau \\ &\text{where}\quad F=P+Q\frac{i}{N} \end{aligned}\right\} \tag{4.20}$$

This is just the equation solved by the analog computer circuit which contains no source of the solution error except the multiplier truncation error.

The solution is expressed as follows.

(i) When $F>0$,

$$\left.\begin{aligned} &Y=S_1\cos\omega(\tau-\tau_i)+S_2\sin\omega(\tau-\tau_i)+C+D\cos\frac{2}{a_t}\tau \\ &\dot{Y}=-\omega S_1\sin\omega(\tau-\tau_i)+\omega S_2\cos\omega(\tau-\tau_i)-\frac{2}{a_t}D\sin\frac{2}{a_t}\tau \end{aligned}\right\} \tag{4.21.1}$$

(ii) When $F=0$,

$$\left.\begin{aligned} &Y=S_1+S_2'(\tau-\tau_i)+C+D\cos\frac{2}{a_t}\tau \\ &\dot{Y}=S_2'-\frac{2}{a_t}D\sin\frac{2}{a_t}\tau \end{aligned}\right\} \tag{4.21.2}$$

(iii) When $F<0$,

$$\left.\begin{aligned} &Y=S_1\cos h\lambda(\tau-\tau_i)+S_2\sin h\lambda(\tau-\tau_i)+C+D\cos\frac{2}{a_t}\tau \\ &\dot{Y}=\lambda S_1\sin h\lambda(\tau-\tau_i)+\lambda S_2\cos h\lambda(\tau-\tau_i)-\frac{2}{a_t}D\sin\frac{2}{a_t}\tau \end{aligned}\right\} \tag{4.21.3}$$

where

$$\left.\begin{aligned} C &= \frac{\dfrac{Q}{0.95}\dfrac{ij}{N^2}}{F} \\ D &= \frac{Q}{0.95}\cdot\frac{i}{N}\left(\frac{4}{a_t^2}-F\right) \\ S_1 &= Y_i - C - D\cos\frac{2}{a_t}\tau_i \\ S_2 &= \frac{S_2'}{\omega} \\ S_2' &= \dot{Y}_i + \frac{2}{a_t}D\sin\frac{2}{a_t}\tau_i \\ \omega &= \lambda = \sqrt{|F|} \end{aligned}\right\} \qquad (4.22)$$

If we denote the multiplier inputs by $x(\tau)$ and $Y(\tau)$ respectively and determine the initial point $(x(0), y(0))$ on the x–y plane and the domain (m, n) where the initial point exists and set $y_i = Y(\tau)|_{\tau=0}$, $\dot{Y}_i = dY/d\tau|_{\tau=0}$, then the solution in a period when the point $(x(\tau), Y(\tau))$ is in (m, n) domain, is given by Eq. (4.21). Now, if the point $(x(\tau), y(\tau))$ comes into an adjoining new domain at $\tau=\tau_i$, we evaluate Y, $\dot{Y}$ in the old domain at $\tau=\tau_i$ and allocate their values to Y_i and $\dot{Y}_i$ for the new domain and determine the values of m, n of the new domain.

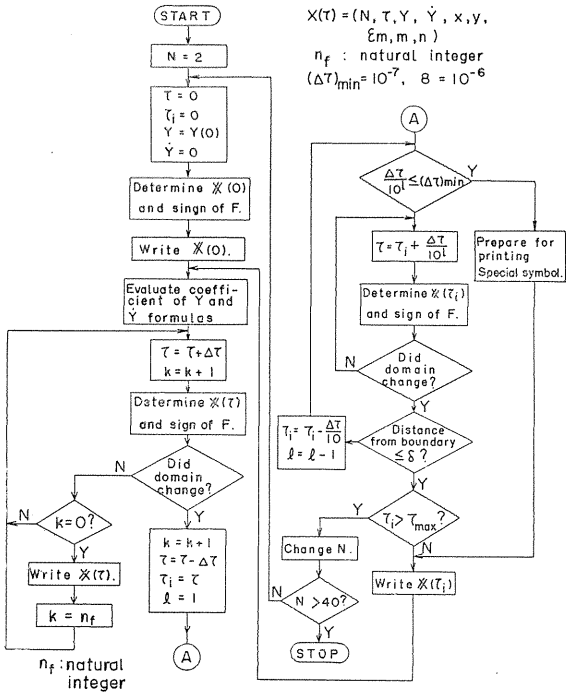

FIG. 4.8. Flow chart for the digital computer simulation of the analog computer circuit of Mathieu equation.

Through this procedure the solution in the new domain is fully determined. The same rule applies after this. Thus we need only to monitor the domain in which the point $(x(\tau), Y(\tau))$ exists and to connect the corresponding solution in succession. Fig. 4.8 shows a flow chart for performing the just mentioned procedure by a digital computer.

(1) Calculation method of m and n

Since the condition under which the point (x, y) exists in (m, n) domain is

$$\left.\begin{aligned} \frac{2m-1}{N} \leq x+y \leq \frac{2m+1}{N} \\ \frac{2n-1}{N} \leq x-y \leq \frac{2n+1}{N} \end{aligned}\right\} \tag{4.22}$$

the inequality determining m, n becomes

$$\left.\begin{aligned} &\overline{m}-1 \leq m \leq \overline{m} \\ &\overline{n}-1 \leq n \leq \overline{n} \end{aligned}\right\} \tag{4.23}$$

where

$$\left.\begin{aligned} \overline{m} &= \frac{1}{2}\{N(x+y)+1\} \\ \overline{n} &= \frac{1}{2}\{N(x-y)+1\} \end{aligned}\right\}$$

Then, if we define m_d, n_d by Eq. (4.24), m, n are given by integer parts of them.

$$\left.\begin{aligned} m_d &= \begin{cases} \overline{m} & (m \geq 0) \\ \overline{m}-1 & (m<0) \end{cases} \\ &\text{Similarly for } n. \end{aligned}\right\} \tag{4.24}$$

This situation is illustrated in Fig. 4.9.

(2) Deviation of the point (x, y) from a boundary line

If the condition

$$\left.\begin{aligned} \| m_d | - | m_0 \| \leq 10^{-5} \\ \| n_d | - | n_0 \| \leq 10^{-5} \end{aligned}\right\} \tag{4.25}$$

is satisfied, where m_0, n_0 represent the old values of m, n, then we regarded the point (x, y) to lie on a boundary line, and allocated to τ_i the value of τ at that time.

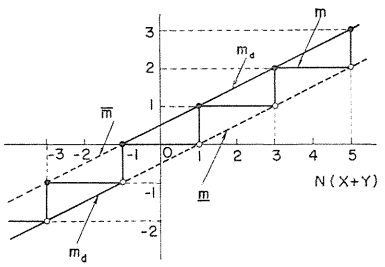

FIG. 4.9. Calculation method of m. (Similarly for n.)

(3) Choice of $\Delta\tau$

When $\Delta\tau$ (refer to Fig. 4.8) is too large, it may be overlooked that the point (x, y) exists in another domain (usually an adjoining domain) through a fraction of $\Delta\tau$.

Here $\Delta\tau=0.01$ was chosen. According to authors' estimation, the magnitude of projection into an adjoing domain is below the order of 10^{-4} and hence suffici-

ently small even in comparison with the side length of the small square domain for $N=20$.

4.2.2. Examples of calculation

Here two representative examples specified by Table 4.1 are dealt with. Example (1) is for the case where Mathieu equation gives a perodic solution $ce_2(z, q)$[23] and thus it is expected that the error of the analog computer solution can be easily observed. Example (2) is a quotation from the examples of numerical calculation in a literature[24]. In this case an unstable solution is obtained and, as the same literature points out, when this equation is solved by the analog computer, the resulting computer solution is very sensitive to the coefficient settings of potentiometers.

TABLE 4.1. Numerical values for the two examples

example	a	q	P	Q	$Y(0)$	$dY(0)/d\tau$	properties of solution
(1)	5.1726651	2	0.64658314	−0.5	1 0.5	0	periodic; $ce_2(a, q)$
(2)	27.8	−15.2	3.475	3.8	0.6	0	stable and non-periodic

This is presumably related to the fact that, in the stable region diagram with a and q as the axises of co-ordinates, the point (a, q) in this case lies near the boundary line between the stable and the unstable regions[24]. That is, example (2) was prepared as a problem: To what degree does the multiplication error due to the truncation error affect on the computer solution, in the circuit where a high accuracy is required of the linear computing elements?

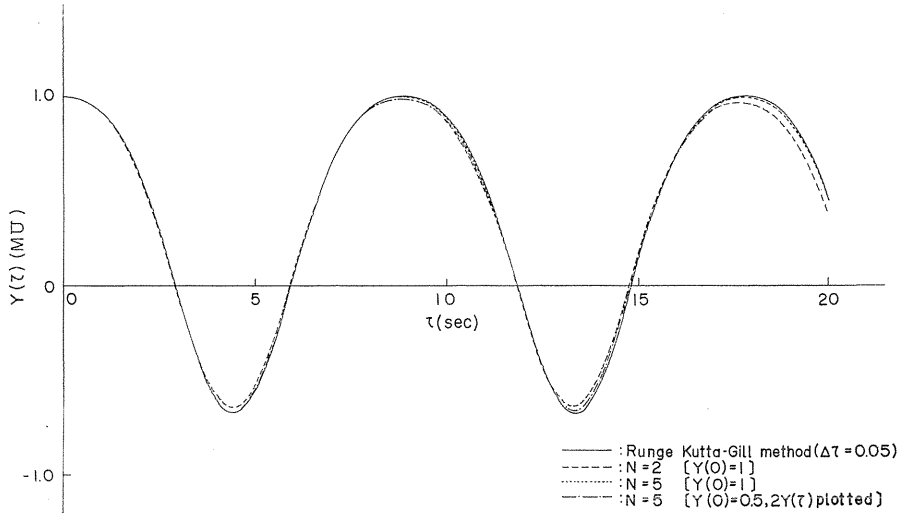

FIG. 4.10. Variation of the solution of Mathieu equation (in periodical case) caused by the piecewise linear approximation error of the diode multiplier (obtained by the digital computer simulation).

(1) Case of the periodic solution

In Fig. 4.10, tne solutions for $N=2$ and $N=5$ and the solution of Eq. (4.17) by Runge-Kutta-Gill method, where a pitch $\Delta\tau$ of τ is 0.05 (we shall later call it *R-K-G* method for short), are plotted together for a ready comparison. We shall consider the solution by *R-K-G* method to be a correct solution, because it is almost perfectly periodic and the difference with a solution for $\Delta\tau=0.1$ is below 3×10^{-6} over one period.

In Fig. 4.10, it should be noted that even if the multiplier has only the static

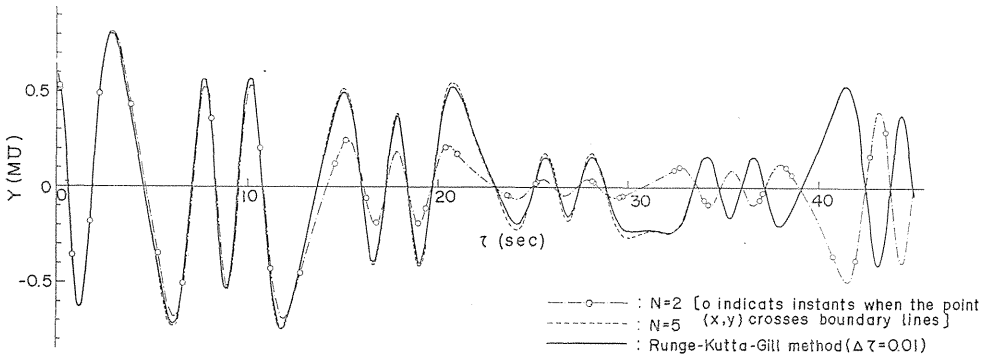

(a) Cases of $N=2$ and $N=5$.

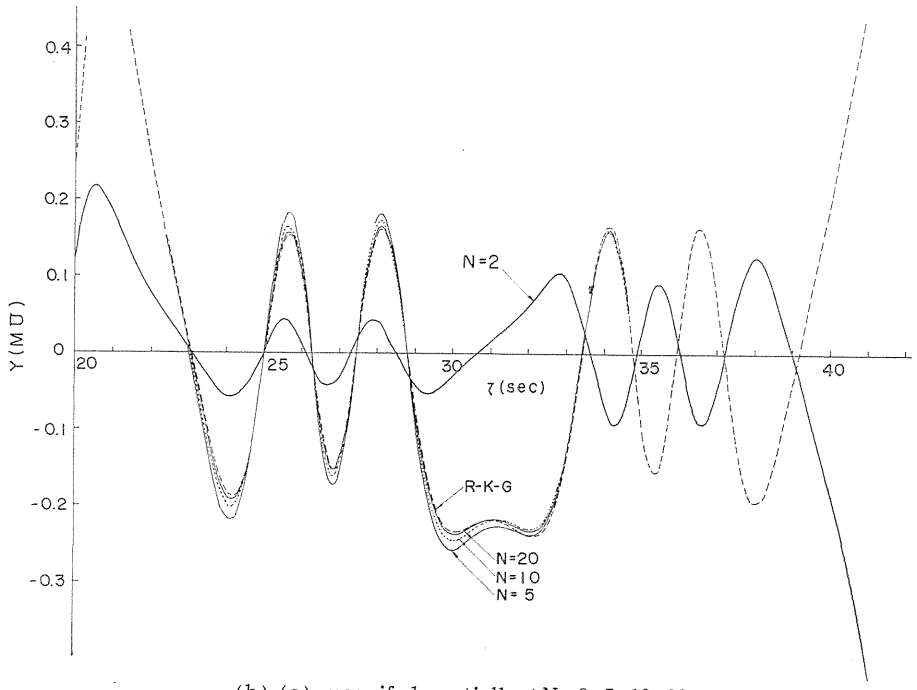

(b) (a) magnifed partially ($N=2$, 5, 10, 20)

FIG. 4.11. Variation of the solution of Mathieu equation (in stable and non-periodic case) caused by the piecewise linear approximation of the diode multiplier (obtained by the digital computer simulation).

error due to the piecewise linear approximation, the variation of solution with time arises.

In the case of $N=5$ in Fig. 4.10, the period and the amplitude decreasing ratio vary in an oscillatory fashion as the operating level of the multiplier, which is performed by adjusting the initial value of Y, increases. This is analogous to the variation of solution period with the solution amplitude given in (4.1.1).

(2) Case of the stable and non-periodic solution

Fig. 4.11 shows the solutions for $N=2$, 5, 10, 20 together with the solution by *R-K-G* method (where $\Delta\tau=0.01$). Here even if $\Delta\tau$ is doubled in *R-K-G* solution, the difference with solution for $\Delta\tau=0.01$ is below the order of 10^{-6} over a whole range illustrated in Fig. 4.11 and thus we consider the solution for $\Delta\tau=0.01$ to be a correct one.

As seen from Fig. 4.11 (a), the solution error for $N=2$ is particularly large and even the main properties of the solution are lost; on the other hand, in the case of $N=5$, the accuracy uaually required of the analog computation is attained. As the theoretical maximum error of the multiplier for this case is $1/(4\times25)=0.01=1(\%)$, the effect of the multiplier error is comparatively small considering that a high accuracy is required of the linear computing elements. Fig. 4.11 (b) is a magnification of a part of (a), where the solution is most sensitive to N.

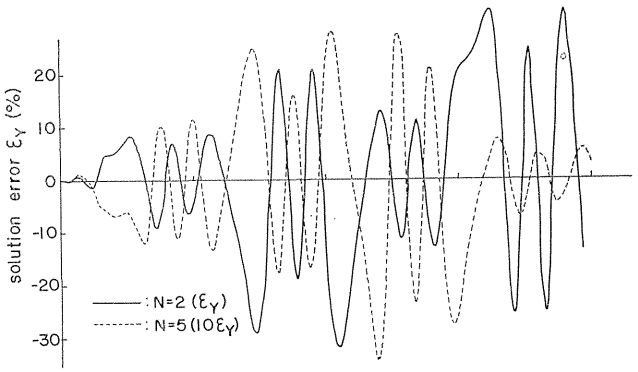

(a) N=2, 5

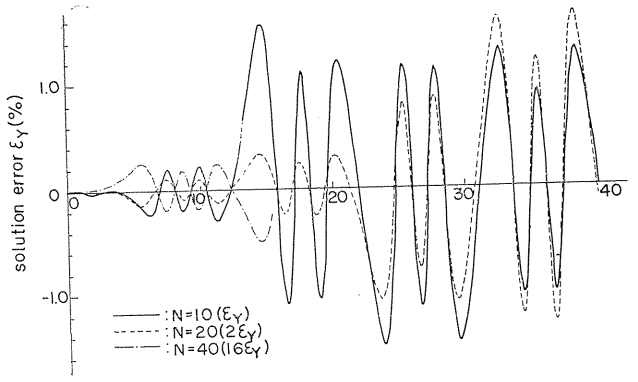

(b) N=10, 20, 40

FIG. 4.12. Variation of the solution error with N.

Here as N increases the solution by digital computer simulation approaches the *R-K-G* solution.

Fig. 4.12 shows the errors contained in the solutions for $N=2$, 5, 10, 20, 40. Here the maximum solution error in the time interval $\tau=0$–12 (sec) is roughly proportional to the theoretical value $1/(4N^2)$ of the maximum multiplication error; in the case of $N=10$, owing to a rapid increase of the solution error near $\tau=12$ (sec), the solution error for larger τ is reduced merely to about one half times the error for $N=5$. Also the solution error for $N=20$ increases rapidly near $\tau=21$ (sec) and the maximum error for larger τ is reduced merely to about one quarter times the value for the case of $N=20$. In summary, although the maximum multiplication error varies as $1/N^2$, the maximum solution error is approximately proportional to $1/N$, unless τ is small. The interpretation of this will be considered below.

4.2.3. Locus of the point (x, y) and its relation to the multiplication error

The error ε_m of the multiplier acts as a forcing function of the differential equation, as shown by a broken line in Fig. 4.7. The instantaneous value of τ is determined by the locus of the point (x, y) moving on $x-y$ plane. Fig. 4.13 shows the locus of the point (x, y) in the case of (4.2.2) (2) together with the small square domains of the multiplier for different values of N.

Now, we assume the velocity of the point (x, y) moving in a small square domain is constant. On this assumption, if the locus of point is paralell to the diagonals of the domain, ε_m has a waveform as shown in Fig. 3.8 and hence the average value of ε_m over a time interval taken by the point to pass through the small square domain, is zero; when the locus of point is parallel to the boundary lines, the average value of ε_m depends on the locus of point.

That is, as shown in Fig. 4.14, when the point goes along the boudary lines with the slopes ± 1, the average values $\bar{\varepsilon}_m$ of ε_m are $\pm(2/3)\cdot\hat{\varepsilon}_m$; when passes through the center of the domain, $\bar{\varepsilon}_m=+(1/3)\cdot\hat{\varepsilon}_m$; and when passes keeping the (shortest) distance of 1/3 times the side length of the domain from the bisector of the domain, $\bar{\varepsilon}_m$ becomes zero. Fig. 4.15 shows a waveform of ε_m for $N=5$; a comparison between this waveform and the locus of the point (x, y) in Fig. 4.13 makes the above-mentioned properties clear. That is, if the point (x, y) goes parallel to boundary lines from domain to domain successively, then the *DC* component of ε_m is strongly dependent on the locus of the point and, in general, its value is rather large. In Fig. 4.13, in the case of $N=10$, the point (x, y) passes along bisetors of small square domains between the times 11.1 (sec) and 11.5 (sec) and hence this may cause almost no solution errors; between the times 12.7 (sec) and 13.9 (sec), however, unfortunatly the point passes along boundary lines, and thus ε_m inclines to large negative values. Furthermore since the variable coefficient $P+Q\cos(2/a_t)\tau$ remains negative through this time interval [12.7–13.9 (sec)], ε_m is cumulatively integrated by the two integrators and the solution error grows rapidly through this period. Since the variable coefficient $P+Q\cos(2/a_t)\tau$ remains negative through this time interval ($\simeq$12.7–13.9), the *DC* component is cumulatively integrated by the two integrators and the solution error increases rapidly.

Now we can say that the above-mentioned phenomenon that even if N is increased from 5 to 10 the solution error is reduced only to about one half, is due

to the fact that the locus of the point (x, y) becomes worse by choosing $N=10$. Moreover, in the case of $N=20$, a rapid growth of the solution error near $\tau=21$ (sec) is attributable largely to the solution error which arised before this time,

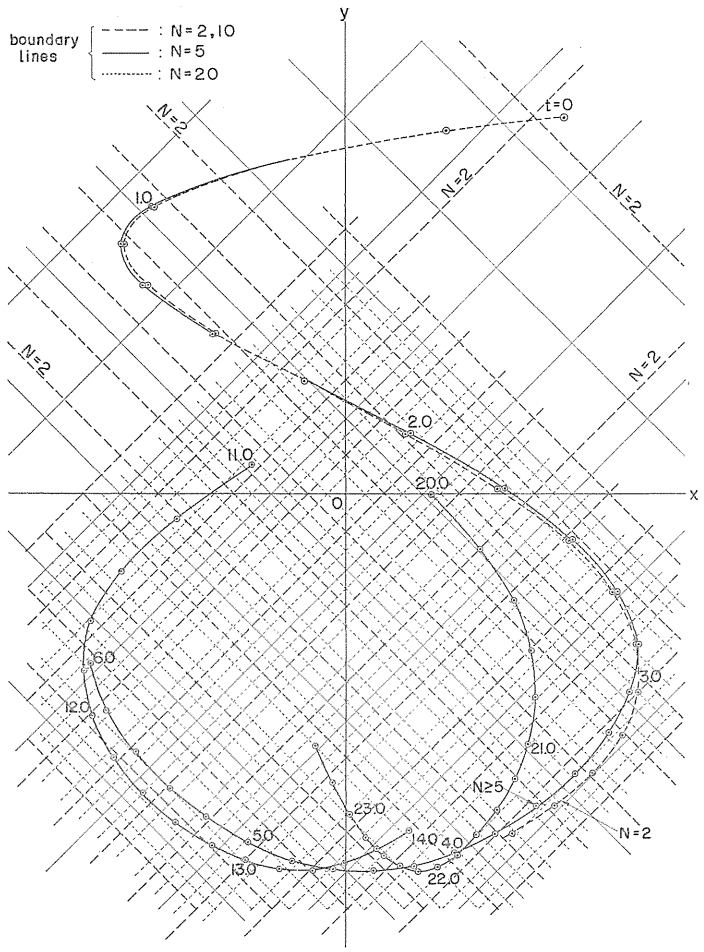

FIG. 4.13. Locus of the point (x, y).

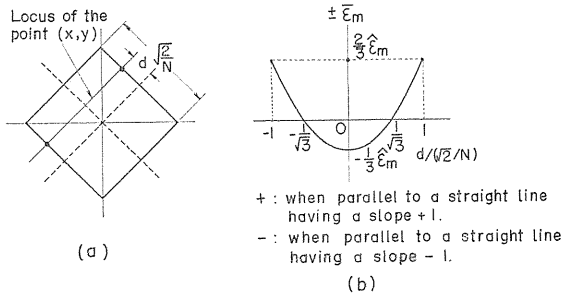

FIG. 4.14. Variation of the mean value $\bar{\varepsilon}_m$ of $\varepsilon_m(\tau)$ with the locus of the point (x, y).

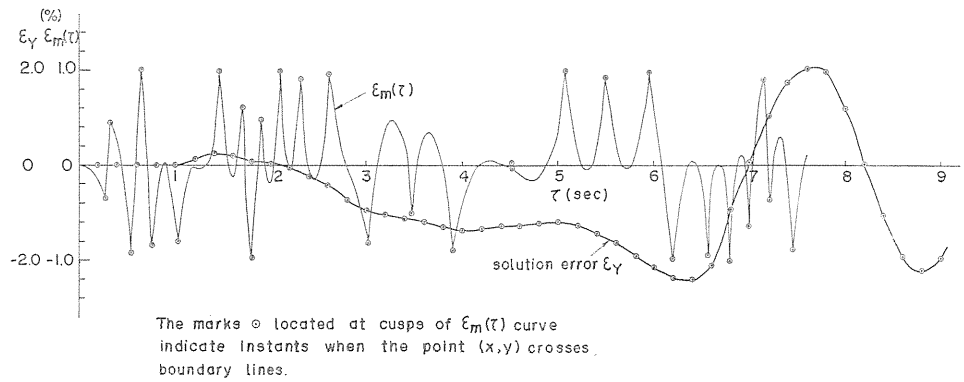

FIG. 4.15. Waveform of $\varepsilon_m(\tau)$ ($N=5$).

and the remaining component of the error is considered to arise from the fact that the point (x, y) passes almost in the boundary lines with the slope -1 through the interval [21.3-22.0] (sec). (Notice that $P+Q\cos(2/a_t)\tau<0$ for $\tau\simeq 21.6$–22.8).

As seen from this, changing the value of N causes not only changes of the minimum and maximum values of the multiplication error as a function of the multiplier two inputs but also the change of the distribution of maxima or minima of the multiplication error, and hence the waveform of the multiplication error ε_m acting as the forcing term of the differential equation to be solved suffers a considerable change, even if its high frequency components are ignored. Presumably, this is the reason why the solution error does not decrease in proportion to $1/(4N^2)$ as N is increased. This phenomena could be observed in solving every differential equation requiring multiplier(s).

If the error reduction factor based on the diode-characteristic is considered, the improvement of solution accuracy as N is increased becomes greater than that derived from the discussion above. Since the form of curved surface of the multiplication error near maxima or minima is round, however, such a probability that the trace of the point (x, y) is unfavorable, is considerably higher and thus in general the solution accuracy could not be improved by the factor $\hat{\varepsilon}_m$ (measured value)/$\hat{\varepsilon}_m$ (theoretical value).

Further, the curved surface of the calibration error $\varepsilon_m(x, y)$ usually may be expected to be fairely smooth and hence it may often happen that the sign of multiplication error remains unchanged for a quite long time. The same applies to the modulation-type multiplier.

4.3. *Explicit solution and implicit solution of the differential equation containing division terms*

As an example, we consider Hill equation described by Eq. (4.26).

$$\frac{d^2y}{dt^2}+\frac{1}{0.5+0.48\cos t}y=0 \tag{4.26}$$

Fig. 4.16 (a) shows the explicit solution of Eq. (4.26) and Fig. 4.16 (b) the alternative solution, namely, the implicit solution of the same equation in which the computer circuit setup are performed after multiplying both the sides of Eq.

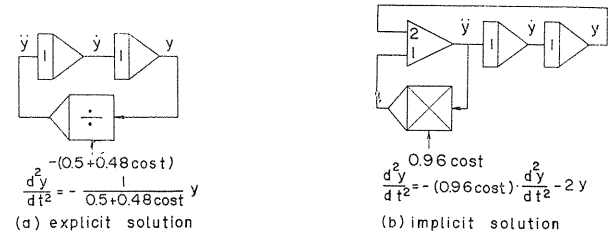

FIG. 4.16. Explicit solution and implicit solution of Hill equation.

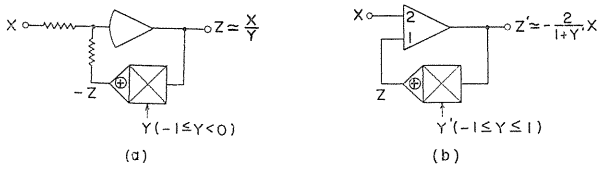

FIG. 4.17. Comparison between the different parts of the explicit solution circuit and the implicit solution circuit.

(4.26) by $(0.5+0.48\cos t)$ for avoiding the use of a divider.

The comparison between the two circuits is reduced to the comparison between Fig. 4.17 (a) and (b), which are parts of the two in which they are different from each other.

4.3.1. Static characteristic

In Fig. 4.17, if

$$Y' = -(1+2Y) \tag{4.27}$$

where X and z denote the input and the output respectively, then (a) and (b) are equivalent.

Since for (a),

$$z = -2X - Z \tag{4.28}$$

and for (b),

$$z = X \tag{4.29}$$

the actual outputs of (a) and (b) can be determined by graphical solution shown in Fig. 4.18. As in Chapter 3, if we denote by $\varepsilon_M(Y)$ the maximum multiplication error in the range $-1 \leq Z(=x) \leq 1$ (where $Y(=y)$ is fixed), then the maximum division error is,

for (a), $$\varepsilon_D(Y) = \frac{\varepsilon_M(Y)}{Y} \tag{4.30}$$

and for (b), $$\varepsilon_D(Y) = \frac{\varepsilon_M(Y')}{2Y} = \frac{\varepsilon_M(-1-2Y)}{2Y} \tag{4.31}$$

If the multiplication error is independent of Y, the error in Fig. 4.17 (a) is half of that in Fig. 4.17 (b) (divider).

In general, however, the multiplier error can be divided into two components: (i) the error which is not significantly dependent on the magnitude of the input, such as the drift in the multiplier output, the piecewise linear approximation error and so on, (ii) the error which decreases as the input $y=Y$ tends to zero, such as the error of multiplication constant, the error caused by the non-linearity of the modulation circuit in the modulation-type multiplier and so on. For (i), (b) is obviously preferable. That is, the disparity between the accuracies of (a) and (b) is at most 1 : 2* and, though in a perfectly adjusted diode multiplier such an improve ment may be expected, it is possible that the relative merits of (a) and (b) are turned in the presence of the error of multiplier constant or in the case where the modulation-type multiplier is used.

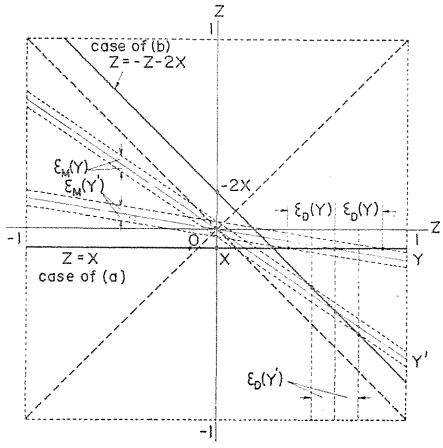

FIG. 4.18. Static error analysis for the circuits of FIG. 4.17 (a) and (b).

4.3.2. Dynamic characteristic

Since the ordinary diode multiplier has nearly the same response characteristic as those of the medium speed linear computing elements, here we deal with the case where the avarage type multiplier or divider represented by the modulation type one is used.

We assume that the dynamic charcteristic of the multiplier can be represented by a linear element connected to the output terminal of the ideal multiplier, such as $k_m(s)$ and $k(s)$ in Fig. 4.19. Here $k(s)$ is the multiplier transfer function with one input fixed, and $K_m(s)$ implies only the phase lag based on modulation principle (From the discussion given later, it is desirable that a low pass filter usually is placed between the summing point and the input terminal of the high gain amplifier, as shown in Fig. 4.19 (a), and therefore this configuration is assumed here).

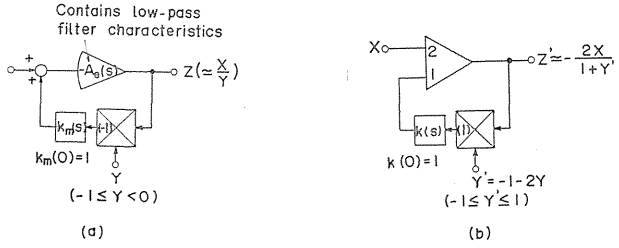

FIG. 4.19. Equivalent circuits for analyzing the dynamic characteristics of the circuits of FIG. 4.17.

* As discussed in Chapter 3, in (a) an output jumping occurres for $0<|Y|<1/N$ and in (b), however, for $0<|Y|<1/(2N)$.

From Fig. 4.19, the output Z is expressed in the following form, by the use of operator symbols defined in Chapter. 2.

$$\left.\begin{aligned} &\text{For (a):} \quad Z = D(Y, s) * \left(\frac{k_m^{-1} * X}{Y}\right) \simeq D_T(Y, s) * \left(\frac{k_m^{-1} * X}{Y}\right) \\ &\text{where} \quad D(Y, s) = \{1 - Y^{-1} \cdot (k_m A_e)^{-1}\}^{-1} \end{aligned}\right\} \tag{4.32}$$

$$\left.\begin{aligned} &\text{for (b):} \quad Z = D'(Y, s) * \left(\frac{k^{-1} * X}{Y}\right) \simeq D_T'(Y, s) * \left(\frac{k^{-1} * X}{Y}\right) \\ &\text{where} \quad D'(Y, s) = \left[1 - Y^{-1} \cdot \frac{1}{2}\{(kA_e)^{-1} + (k^{-1} - 1)\}\right]^{-1} \end{aligned}\right\} \tag{4.33}$$

Here $D_T(Y, s)$ and $D_T'(Y, s)$ are the amplitude-phase modulation operators based on the approximate interpretation of (2.5.2).

The difference between the characteristics of (a) and (b) can be clearified by comparing the frequency characteristics of $D_T(Y, j\omega)$ and $D_T'(Y, j\omega)$.

Fig. 4.20 (a) shows the frequency characteristic of a triangular-wave multiplier or divider, which is a typical example of avarage type multiplier or divider.

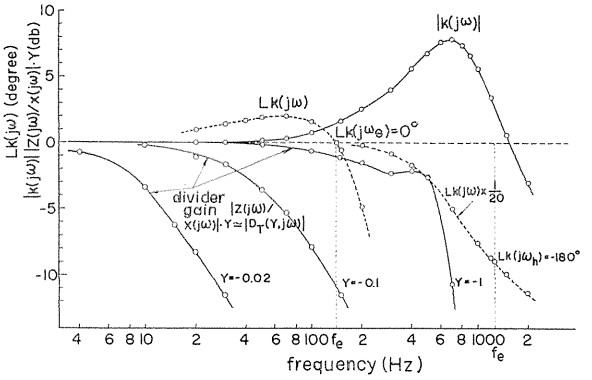

(a) Example of the frequency characteristics of the triangular-wave multiplier/divider (measured).

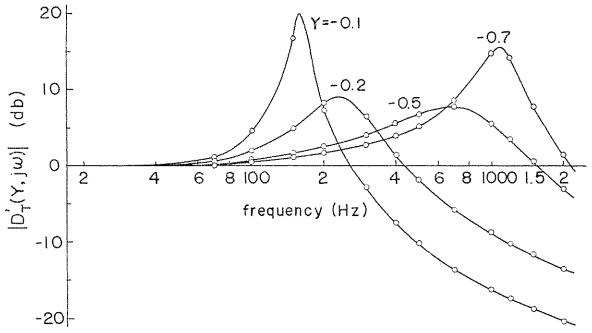

(b) Frequency characteristic of $|D_T'(Y, j\omega)|$ derived from (a).

FIG. 4.20. Comparison between $|D_T(Y, j\omega)|$ and $|D_T'(Y', j\omega)|$.

The frequency characteristic of the divider in the case where X is regarded as an input and Z an output and Y a parameter, is given by $D_T(Y, j\omega)$, if the effect of $k_m(j\omega)$, which is small enough in this example, may be ignored. On the other hand, calculating and plotting $D'_T(Y, j\omega)$ from the characteristic of $k(j\omega)$ in Fig. 4.20 (a) assuming $(kA_e)^{-1} \simeq 0$ leads to Fig. 4.20 (b). The smaller $|Y|$ is, at the lower frequency the $|D_T(Y, j\omega)|$ curve begins to fall; on the contrary, $|D'_T(Y, j\omega)|$ has a sharp peek near 160 (Hz) when $|Y|$ is small and this is essentially different from the divider characteristic.

This phenomena springs from the fact that $|k(j\omega)|$ has a distinctive frequency characteristic as shown in Fig. 4.20, although it is common in the average type multipliers. That is, by the hump characteristic for avoiding phase lag in low frequencies, usually an angular frequency ω_l such that $\angle k(j\omega_l) = 0$ exists, and $|k(j\omega_l)| > 1$ at ω_l; and hence, since the gain round the loop containing the multiplier in Fig. 4.19 (b) is $-Y'k(j\omega)$, the positive feedback of the loop gain more than unity takes place and an oscillation results. On the other hand, although the feedback is negative in low frequency region for $Y' > 0$, the unstability in high frequency region occurs for $|k(j\omega_h)|^{-1} \leq Y' \leq 1$, provided $k(j\omega_h) \geq 1$ at the angular frequency ω_h such that $\angle k(j\omega_h) = -180°$. Correspondingly, in the graph of $|D'_T(Y, j\omega)|$ a peak appears near ω_l and increases in height as Y' approaches $-|k(j\omega_l)|^{-1} (\fallingdotseq -1)[Y \to (|k(j\omega_l)|^{-1} - 1)/2 \simeq 0]$; on the other hand, a peak appears near ω_l and increases gradually in height as Y' tends to $|k(j\omega_l)|^{-1}[Y \to -(1 + |k(j\omega_h)|^{-1}])$. When we have $Y' = 0$ $(Y - 1/2)$ as an intermidiate condition, $|D'_T(Y, j\omega)|$ has a flat characteristic.

Consequently it may be expected that the response speed of (b) is much higher than that of (a), because the frequency characteristic curve of $D'_T(Y, j\omega)$ has a peak. However, a ringing may arise in the divider output when $(k^{-1} \cdot X)/Y$ a great deal of high frequency components, although it occurs rarely.

4.3.3. Experimental results concerning the dynamic characteristics

Fig. 4.21 is a comparison between those outputs of the two circuits (a) and (b) which were observed when the inputs of the two circuits were so chosen that both the two will produce the same output in an ideal case. (In this experiment, since an oscillation occurs when Y' approaches -1 if the multiplier has the characteristic of Fig. 4.20 (a), the multiplier was so adjusted that the phase advance in low frequency region is small and hence ω_l is small.)

Fig. 4.21 (1) is the case of $\omega = 25$ (rad/sec) in the divider; because of poor rise up speed for small divisors, the maximum value is no more than about one half of the correct value 1 (MU). For the circuit of Fig. 4.17 (b), however, even for the same value of ω no decrease of maximum of output values is observed [Fig. 4.21 (2)]. As ω is increased, nevertheless, a ringing appears after the undershoot [Fig. 4.21 (3) or (4)]. These facts have a good agreement with the results by the theoretical consideration mentioned above.

4.4. An improving method of divider accuracy by amplifying the dividend and the divisor inputs by the same factor

An increase of division error (whether static or dynamic) occurs when the divisor is small; therefore, on this occasion, if the divisor and the dividend signals are given the divider after being amplified by the same factor, the division accuracy will be improved.

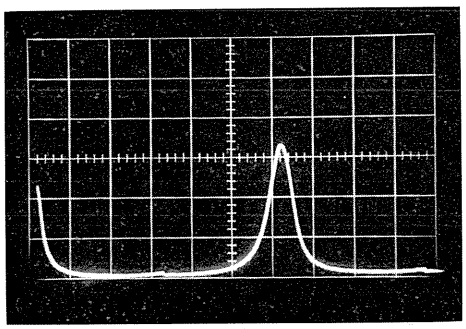

(1) Circuit (a) (divider), $\omega=25$ (rad/sec).

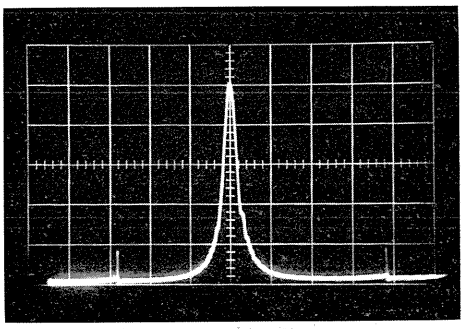

(2) Circuit (b), $\omega=25$ (rad/sec).

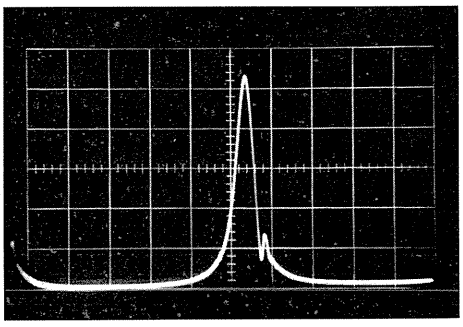

(3) Circuit (b), $\omega=50$ (rad/sec).

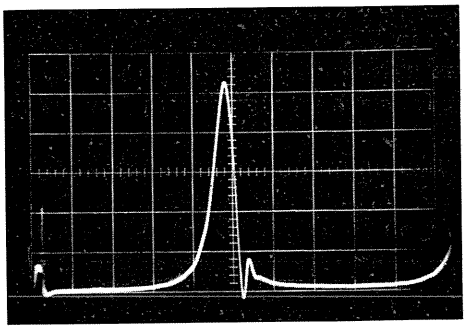

(4) Circuit (b), $\omega=100$ (rad/sec).

Ordinates: 0.2 (MU/div)

FIG. 4.21. Comparison between the dynamic characteristics of the circuits in FIG. 4.19 (a) and (b) (Output waveforms of the triangular-wave multiplier/divider in the case when $X=-0.02$, $Y=-(0.5+0.48\cos\omega t)$ and $Y'=0.96\cos\omega t$.)

4.4.1. Principle

First we consider the general case where the elements A and B having the input-output characteristics $f_1(Y)/Y$ and $f_2(Y)/Y$ respectively are connected to the input terminals of the divider, as shown in Fig. 4.22. In this figure, if $f_a(Y)=f_b(Y)\equiv f(Y)$, that is, the characteristics of A and B are similar in mathematical meaning, we have

$$X_n/Y_n=X/Y \tag{4.34}$$

Here if A an B have a characteristic like that of divider, the function $f(Y)$ is weakly dependent on Y and hence the dynamic range of the divisor input $[Y_n=f_b(Y)]$ of divider is much narrower than that of Y and the improvement of division accuracy can be attained. If $f(Y)$ is constant, however, A and B imply the ideal dividers and thus this method is meaningless. The method in Fig. 4.23 (a)

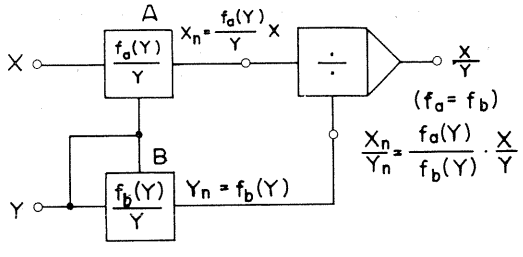

FIG. 4.22. A method for improving the division accuracy which consists in amplifying the divisor and the dividend signals by the same factor.

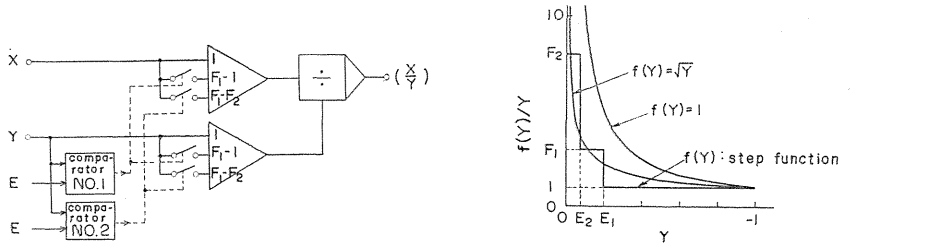

(a) Discontinuous coefficient switching (f(Y)/Y : step function).

(b) Examples of input-output characteristic of the elements A and B

FIG. 4.23. Actual example of the method of FIG. 4.23.

is based on a stairs-like approximation of $f(Y)/Y$ and if this is realized by switching the input coefficients of summing amplifiers, an close similarity between A and B may be expected. However, as this involves discontinuous changes of amplification factors, we must consider below the effects of transient phenomena which become important when the average-type multiplier or divider used.

4.4.2. Transient phenomena in the average-type multiplier or divider

In the dynamic equivalent circuit in Fig. 4.19 (a), we consider the case when

$$\left.\begin{aligned} X &= X_0 + (F-1)X_0 \cdot u(t) \\ Y &= Y_0 + (F-1)Y_0 \cdot u(t) \end{aligned}\right\} \tag{4.35}$$

where X_0, Y_0 are constant and F an amplification factor.

Here if the effect of $k_m(s)$ cannot be ignored, then the waveforms of $k_m^{-1} * X$ and X, as seen from Eq. (4.32), is not similar, so that spikes appears in the output waveform. On the other hand, if $k_m(s) \simeq 1$ in connection with the discussion in (2.5.1), we have

$$\left.\begin{aligned} Z &= Z_1 + \{1-(FY_0A_{e0})^{-1}\}D(FY_0) * (Z_2 - Z_1)u(t) \\ \text{where} \quad D(FY_0) &= [1-\{FY_0A_e(s)\}^{-1}]^{-1} \end{aligned}\right\} \tag{4.36}$$

In this place Z_1 and Z_2 denote the steady state divider outputs before and after the coefficient switching respectively, and we obtain the following:

$$\left.\begin{aligned} Z_2 - Z_1 &= -\frac{1}{1-(A_{e0}FY_0)^{-1}} + \frac{1}{1-(A_{e0}Y_0)^{-1}} \\ &\simeq (A_{e0}Y_0)^{-1} - (A_{e0}FY_0)^{-1} \end{aligned}\right\} \tag{4.37}$$

As the two terms in the second right hand member of Eq. (4.37) are the inverses of the *DC* loop gains of the divider before and after switching and thus sufficiently small, no appreciable transient phenomena may occur in Z of Eq. (4.36).

4.4.3. An experiment

Fig. 4.24 is a computer circuit for Eq. (4.38) which is Hill equation with a forcing term added, where the coefficent switching is taken place.

$$\frac{d^2y}{dt^2} + \frac{1}{0.5+0.48\cos t}y = 0.2\cos t \tag{4.38}$$

This equation gives a periodic solution, if the initial condition is chosen so that

$$\left.\begin{aligned} y_{t=0} &= 0.6424 \\ (dy/dt)_{t=0} &= 0 \end{aligned}\right\} \qquad (4.39)$$

This periodic solution by the series solution is graphed in Fig. 4.25.

Without switching, it was observed experimentally that the computer solution is very sensitive to the choice of time scale factor and to the adjustment condition of multiplier or divider and therefore it is considered that the solution of Eq. (4.38) is strongly affected by the static and the dynamic errors of divider; however, if the switching method used, the solution accuracy is largely improved as shown in Fig. 4.26 (b).

Moreover, possibly those spikes accompanied by $D-1$ output waveform which correspond to the coefficient switching, are caused by the descripancy between the operating times of the switches for divisor and dividend and by the fact that the dynamic characteristic of multiplier can not exactly be expressed by the equivalent circuit in Fig. 4.19 (a).

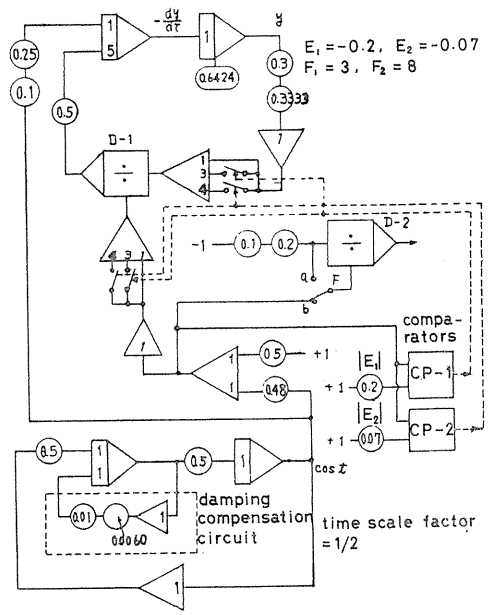

FIG. 4.24. Analog computer circuit for Eq. (4.38) subjected by the initialcondition given by Eq. (4.39), where three stages coefficient switching is taken place.

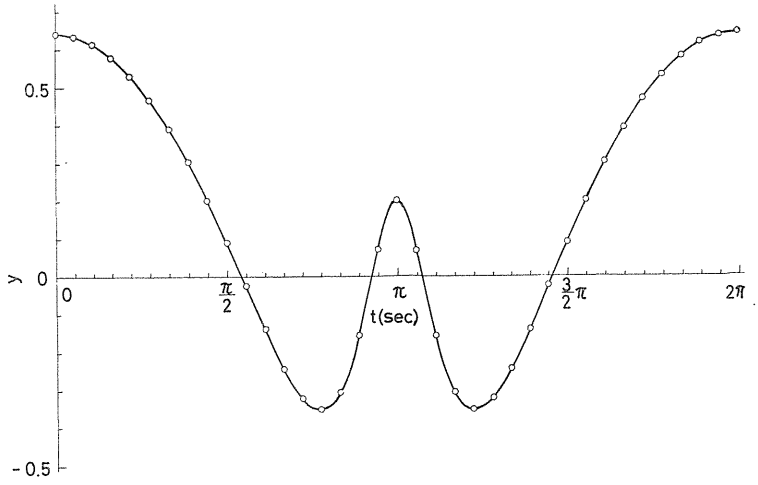

FIG. 4.25. Periodic solution curve of Eq. (4.38) (by the series solution).

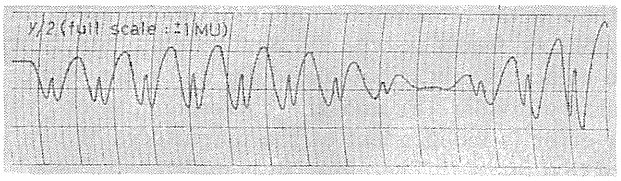

(a) Case without the coefficient switching.

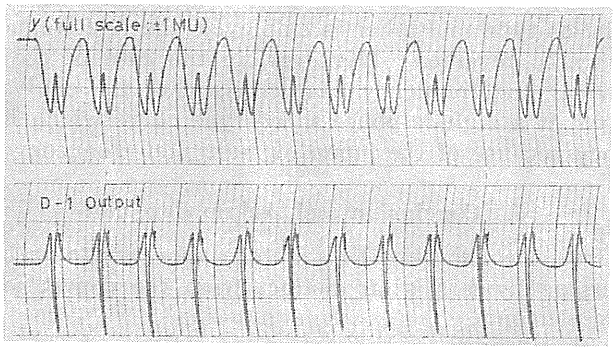

(b) Case when the coefficient switching was taken place.
FIG. 4.26. Experimental results.

4.5. Conclusion of chapter 4

In summary, the studies of this chapter are as follows.

(1) In the circle test circuit in which the diode multiplier with one input held constant or the corresponding diode divider with divisor input constant is inserted, the solution periode is strongly dependent on the solution amplitude because of the truncation error, especially in a range where the solution amplitude is small. This phenomena were analysed by describing-function method and the results were proved by experiment.

(2) The analog computer circuit for Mathieu equation which contains the diode multiplier was simulated by the digital computer considering only the truncation error, and the relation between the number N of breakpoints per quadrant and the solution error was investigated for two cases of (1) periodic solution and (2) nonperiodic solution.

From the results for (1), we found that in a variable coefficient differential equation the periodicity of solution can be violated even by the truncation error of the multiplier which is a kind of static errors. From the simulation for (2), it was clearified that the solution error does not necessarily decrease in proportion with the maximum error $1/(4N^2)$ of the multiplier as N is increased. The reason for this is as follows: when N is changed, not only the extremum value $1/(4N^2)$ of multiplication error changes but also the distribution of extremum points changes, and therefore a functional form of the multiplication error $\varepsilon_m(\tau)$ which acts as a forcing function to the original equation varies in complexity with N, so that the effect of $\varepsilon_m(\tau)$ on the solution does not necessarily decrease smoothly as N is increased.

(3) In solving a differential equation containing one or more division terms, if we choose the implicit solution instead of the explcit solution for avoiding the

use of divider, then in the resulting computer circuit the equivalent divider circuit similar to the ordinary feedback-type divider appears and hence the difference between the two solutions is attributable to the difference between the characteristics of the ordinary divider (a) and the corresponding equivalent divider (b). If the multiplier error is independent of the magnitudes of two inputs, the error of (b) is a half of that of (a). Therefore, in completely adjusted diode multiplier, an accuracy improvement factor near this can be expected. However, when there is some error in adjustment in the multiplication constant of diode multiplier or when the modulation-type multiplier is employed, the relative merits between the two solutions may be reversed. Moreover, in the case of the modulation-type multiplier or divider, the frequency characteristic of the equivalent divider for small divisor input is a high response speed type curve which has a hump at a medium frequency because of the hump of multiplier frequency characteristic.

5. Conclusion and Acknowlegemant

As is clear from the discussion thus far, the approach to problems concerning analog multipliers or dividers is far distinct from the conventional approach to linear computing elements.

Although with this approach the basic problems which are important for analog computer designers and users have been almost throughly studied, related problems as below are remained for future investigation.

In this paper a main use of diode multipliers or dividers was assumed to be in ordinary analog computers and hence the dynamic characteristic not dealt with. Recognizing that diode multipliers are also used in ultra high speed computing circuits for their high speed response, however, ignoring a detailed dynamic characteristic analysis based on high frequency characteristics of diodes, resistors and other elements, can not necessarily be justified.

As to Chapter 4, futher the following matters are to be considered: (1) the relation between the solution errors in the circle test circuit and the Mathieu equation solving circuit, (2) the details of the solution error in computer circuits including one or more (diode) dividers, (3) the effect of equally amplifying dividend and divisor in diode multipliers or divides.

For (1), since in circle test circuit the diode multiplier operates in one-dimensional manner while in the Mathieu equation solving circuit in two dimansional manner, some relation between the solution errors of the two cases could be expected. But at present no details of this are known. In (3), if we consider that the diode divider possesses a jagged error surface, it is expected that the effect of division error on the computer solution is very sensitive to the coefficient switching time.

(4) For the case where the amplification factors for divisor and dividend inputs are changed discontinuously, it was shown that under the condition that the effect of $k_m(s)$ can be ignored, even if the average-type multiplier or divider with a comparatively narrow frequency band width is employed, the transient phenomena occuring at an instance of the coefficient switching are neglesibly small; and this has been proved by experiment.

In this paper, the digital computer simulations of analog computer circuits and the related numerical calculations were performed by NEAC 2203 and the other numerical calculations by FACOM 270-10.

In concluding, the authors wish to thank Mr. G. Sugimoto and Mr. Y. Takeichi for their earnest cooperation in the course of this study.

Moreover, this work was supported financially by a scientific research grant of the Ministry of Education and the Sakkokai foundation.

References

1) R. Tomovic and W. J. Karplus: High Speed Analog Computers, p. 115, John Wiley, 1962.
2) Yamashita: Electronic Computers, pp. 262-265, 1959; Ichikawa, Yokoi, Miyake, and Takabayashi: Trans. of the 1960 Tokai Branch Joint Conv. of the Four Elec. Insts., Japan, 33; Otoba, Shibatani, and Kuwata: Trans. of the 1961 Joint Conv. of the Four Elec. Insts., Japan, 299; Abe: Papers presented at the Technical Group on Analog Techniques, **1**, 21, 1962; Inagaki and Arajo: Papers presented at the Technical Group on Analog Techniques, **3**, 1, 1963; Inagaki, Furuta, and Arajo: Papers presented at the Technical Group on Analog Techniques, **4**, 1, 1964.
3) T. Nomura and T. Miura: Electronic Analog Computers, p. 250, Corona Co., Japan, 1960.
4) Numakura: J. of I.E.E., Japan, **80**, 896, 1960.
5) M. Ichikawa and Y. Miyake: Journal of the Society of Instrument and Control Engrs, **1**, 853, 1962.
6) Y. Miyake and M. Ichikawa: Papers presented at the Technical Group on Analog Techniques, **3**, 17, 1963.
7) Y. Miyake and M. Ichikawa: Papers presented at the Technical Group on Analog Techniques, 2, 1, 1962.
8) Y. Miyake and M. Ichikawa: Trans. of the 1962 Tokai Branch Joint Conv. of the Four Elec. Insts, Japan, 41.
9) Y. Miyake and M. Ichikawa: Trans. of the 1963 Joint Conv. of the Four Elec. Insts, Japan, 373.
10) Y. Miyake and M. Ichikawa: Trans. of the 1963 Tokai Branch Joint Conv. of the Four Elec. Insts., Japan, S-2-10.
11) Y. Miyake and M. Ichikawa: Trans. of the 1964 Joint Conv. of the Four Elec. Insts., Japan, 353.
12) Y. Miyake and M. Ichikawa: J. of I.E.E., Japan, 85, 1926, 1965.
13) Y. Miyake: Papers presented at the Technical Group on Analog Techniques, **6**, 5, 1966.
14) Y. Miyake, M. Ichikawa, and G. Sugimoto: Trans. of the 1967 Joint Conv. of the Four Elec. Insts., Japan, 2976.
15) Y. Miyake and G. Sugimoto: Journal of the Central Japan Society of Automatic Control Engrs, **10**, 1, 38, 1967.
16) Y. Miyake, G. Sugimoto and M. Ichikawa: Trans. of the 1967 Tokai Branch Joint Conv. of the Four Elec. Insts., Japan, 4 a-D-2.
17) R. Abe and T. Wakui: Papers presented at the Technical Group on Analog Techniques, 8, 1, 1968.
18) R. Abe and T. Wakui: Trans. of the 1968 Joint Conv. of the Four Elec. Insts., Japan, 3331.
19) Y. Miyake and M. Ichikawa: Trans. of the 1968 Joint Conv. of the Four Elec. Insts., Japan, 2701.
20) Y. Miyake and M. Ichikawa: Trans. of the 1969 Joint Conv. of the Four Elec. Insts., Japan, 3331.
21) Y. Miyake, Y. Takeichi, and M. Ichikawa: Trans. of the 1970 Joint Conv. of the Four Elec. Insts., Japan, 2925.
22) Y. Sawaragi *et al.*: Automatic Control Theory, Kyoritsu Shuppan Co., Japan, 1962.
23) N. W. Mclachlan: Theory and Application of Mathieu Functions, Dover Publications Inc., 1964.

24) S. Hayashi and K. Mizukami: J. of I.E.E., Japan, 86, 603, 1966.
25) Y. Miyake and M. Ichikawa: Trans. of the 1968 Tokai Branch Joint Conv. of the Four Elec. Insts., Japan, 9 a-F-5.
26) G. A. Korn and T. M. Korn: Electronic Analog and Hybrid Computers, McGraw-Hill Book Co., 510, 1964.
27) L. Bauer: Aircraft, Autopilot and Missile Problems, Computer Handbook edited by H. D. Husky and G. A. Korn, pp. 5-61 to 62, McGraw-Hill Book Co., 1962.
28) Y. Miyake and M. Ichikawa: Trans. of the 1966 Joint Conv. of the Four Elec. Insts., Japan, 1962.